

DIELECTRIC PROPERTIES OF $\text{CaCu}_3\text{Ti}_4\text{O}_{12}$
AND ITS RELATED MATERIALS

A Thesis

Presented to

The Graduate Faculty of The University of Akron

In Partial Fulfillment

of the Requirement for the Degree

Master of Science

Yang Sun

August, 2006

DIELECTRIC PROPERTIES OF $\text{CaCu}_3\text{Ti}_4\text{O}_{12}$
AND ITS RELATED MATERIALS

Yang Sun

Thesis

Approved:

Accepted:

Advisor
Dr. Ang Chen

Dean of the College
Dr. Ronald Levant

Faculty Reader
Dr. Jun Hu

Dean of the Graduate School
Dr. George Newkome

Faculty Reader
Dr. Alper Buldum

Date

Department Chair
Dr. Robert Mallik

ABSTRACT

Dielectric materials have been widely used in electronic industry. Recently an oxide ceramic $\text{CaCu}_3\text{Ti}_4\text{O}_{12}$ (denoted as CCTO) is reported to be very promising because it possesses a very high dielectric constant. However, further research on its dielectric properties indicates that this material has a high dielectric loss, which seriously blocks its practical application.

In this work, pure CCTO ceramic, and two series of CCTO derivatives, i.e., “CCTO + CaTiO_3 ” and “CCTO + MnO_2 ” ceramics were prepared, and their phase assemblies, structure, dielectric properties, and conducting properties are studied.

The results show that CCTO is single phase perovskite structure, and at room temperature, it exhibits a dielectric constant of ~ 18400 and a dielectric loss of ~ 0.115 at 1 kHz; its resistivity is 219 $\text{k}\Omega\text{cm}$ at 295 K. This means that although the pure CCTO has a huge dielectric constant, it is not a good dielectric material for making capacitors due to its high dielectric loss and low resistivity.

Incorporating with CaTiO_3 (CTO) or doped with MnO_2 additive effectively decreases the dielectric loss of CCTO. For example, at a CTO volume ratio of 0.5, the dielectric loss maximum is reduced from to 2.72 to 0.7 at 1 kHz while its dielectric constant is reduced from 15286 to 3831 at 200K. In CCTO doped with MnO_2 , the dielectric constant is dramatically decreased from 15286 for pure CCTO to 1831 for the

sample doped with 1% MnO_2 , and the dielectric loss is also greatly suppressed from 0.0447 to 0.0158 at 200K. This indicates that these methods are promising ways to improve the dielectric performance of CCTO-based materials for a possible practical application.

The relaxation mechanism was investigated for CCTO and its derivatives. It is for the first time revealed that the relaxation time follows the Vogel-Fulcher relation instead of the Arrhenius relation.

ACKNOWLEDGEMENTS

I would like to express my sincere thanks to Dr. Ang Chen, my advisor, for all his guidance and encouragement that he provided in the course of this research work at The University of Akron. I am grateful for his time, patience and consideration.

I would also like to thank Dr. Yu Zhi for her help during my research. Her careful amendments and creative ideas are greatly appreciated.

In addition, I would also like to thank my committee members, Dr. Alper Buldum and Dr. Jun Hu for their patience and helpful instructions. My thanks also go to all faculty members of the Physics Department and to Mr. Gregg Allen and Ms Theresa Yost for their help throughout the course of this study.

My thanks will not be complete until I acknowledge my colleague and friend Yuan Zhou who sacrificed a lot of her time to help with my experiments. My sincere thanks also go to Mr. Tom Quick, the technician of Geometry, for his assistance on XRD experiments.

Lastly, I would like to thank my parents, my uncle and aunt for their love and encouragements.

TABLE OF CONTENTS

	Page
LIST OF TABLES.....	viii
LIST OF FIGURES.....	ix
CHAPTER	
I INTRODUCTION.....	1
1.1 Background of $\text{CaCu}_3\text{Ti}_4\text{O}_{12}$	1
1.2 Intrinsic behavior of $\text{CaCu}_3\text{Ti}_4\text{O}_{12}$	3
1.3 Doping methods.....	7
II EXPERIMENTAL PROCEDURE.....	10
2.1 Sample Preparation.....	10
2.1.1 compositions.....	10
2.1.2 Weighing and mixing.....	11
2.1.3 Calcining.....	11
2.1.4 Pressing.....	12
2.1.5 Sintering.....	12
2.2 Structure and density examination.....	12
2.2.1 Density Measurement.....	12
2.2.2 X-ray Diffraction examination.....	13
2.3 Dielectric and electrical properties measurements.....	13
2.3.1 Dielectric properties measurements.....	13

	2.3.2 Electrical properties measurements.....	14
III	EXPERIMENTAL RESULTS.....	16
	3.1 Pure $\text{CaCu}_3\text{Ti}_4\text{O}_{12}$ ceramics.....	16
	3.2 $\text{CaCu}_3\text{Ti}_4\text{O}_{12}$ incorporating with CaTiO_3	20
	3.3 CCTO doped with MnO_2	25
IV	DISCUSSION.....	33
	4.1 Pure $\text{CaCu}_3\text{Ti}_4\text{O}_{12}$	33
	4.1.1 Introduction.....	33
	4.1.2 Cole-Cole plot analysis.....	33
	4.1.3. Relaxation times.....	35
	4.2 $\text{CaCu}_3\text{Ti}_4\text{O}_{12}$ doped with CaTiO_3	37
	4.2.1. Characterization of $\text{CaCu}_3\text{Ti}_4\text{O}_{12}$ doped with CaTiO_3	37
	4.2.2 structure examination by X-ray diffraction.....	39
	4.2.3 Cole-Cole plot analysis of $(1-y) \text{CaCu}_3\text{Ti}_4\text{O}_{12} + y \text{CaTiO}_3$ (volume ratio $y=0.5, 0.8$ and 0.9).....	41
	4.2.4 Relaxation Discussion.....	44
	4.2.5 Lichtenecker's Logarithmic Law.....	44
	4.3 $\text{CaCu}_3\text{Ti}_4\text{O}_{12}$ doped with MnO_2	46
	4.3.1. Characterization of $\text{CaCu}_3\text{Ti}_4\text{O}_{12}$ doped with MnO_2	46
	4.3.2. Cole-Cole plot analysis of $\text{CaCu}_3\text{Ti}_4\text{O}_{12}$ with MnO_2 additive.....	46
V	CONCLUSIONS.....	49
	5.1 Study of pure $\text{CaCu}_3\text{Ti}_4\text{O}_{12}$	49
	5.2 Study of $(1-y) \text{CaCu}_3\text{Ti}_4\text{O}_{12} + y \text{CaTiO}_3$ ($y= 0.5, 0.8, 0.9$).....	49

5.3 Study of $\text{CaCu}_3\text{Ti}_4\text{O}_{12} + z \text{MnO}_2$ ($z = 0.01, 0.02, 0.03, 0.04, 0.05$).....	50
5.4 Summary.....	51
REFERENCES.....	52

LIST OF TABLES

Table	Page
1.1 Effects of Co, Ni, Fe doping in CCTO material.....	9
2.1 Purity level of the raw reagents.....	10
2.2 Parameters used in X-ray diffraction measurement.....	13
3.1 Density measurements of CCTO samples.....	16
3.2 Dielectric properties of (1-y) CCTO – y CTO.....	21
3.3 Height of ϵ shoulder and $\tan\delta$ peak for different MnO_2 compositions at 1 kHz...32	
4.1 Fitting results of Cole-Cole plot of (1-y) $\text{CaCu}_3\text{Ti}_4\text{O}_{12} + y\text{CaTiO}_3$ volume ratio y=0.5, 0.8 and 0.9.....	42
4.2 Dielectric constant of CCTO-CTO at 295K for 1 kHz.....	45
4.3 Fitting results of Cole-Cole plot for CCTO with different MnO_2 concentration..	47

LIST OF FIGURES

Figure	Page
1.1 crystal structure of CCTO shown as TiO ₆ octahedral, Cu atoms bonded to four oxygen atoms, and large Ca atoms without bonds.....	2
1.2 (a) The temperature-dependence of the real part of the dielectric response of CCTO, at different frequencies between 100 and 1MHz. (b) The loss component of the dielectric response at the same frequencies.....	4
1.3 Polarized Raman spectra of CCTO at room temperature.....	4
1.4 Impedance complex plot, Z at (a) 300k and (b) 104,115 and 130k, for CCTO ceramics. The inset in (a) shows an expanded view of the high frequency data close to the origin. Filled symbols indicate selected frequencies in Hz.....	5
1.5 SEM images of ceramic microstructure for CCTO ceramics sintered at 1100C for a) 3h and b) 24h.....	7
2.1 The dark parts are covered with electrodes and are each connected to a cable.....	15
3.1(a), (b) Dielectric constant and dielectric loss of pure CCTO.....	18
3.2 Dielectric constant and loss vs. temperature	19
3.3 Resistance measurement of pure CCTO.....	19
3.4 Conductivity for pure CCTO.....	20
3.5 (a) (b) Dielectric constant and dielectric loss of material 0.5CCTO+ .5CTO.....	22
3.6 (a) (b) Dielectric constant and dielectric loss of material 0.2CCTO+0.8CTO.....	23
3.7 (a) (b) Dielectric constant and dielectric loss of material 0.1CCTO+0.9CTO.....	24
3.8 (a) (b) Dielectric constant and dielectric loss of material CCTO doped	

with 1% MnO ₂	26
3.9 (a) (b) Dielectric constant and dielectric loss of material CCTO doped with 2% MnO ₂	27
3.10 (a) (b) Dielectric constant and dielectric loss of material CCTO doped with 3% MnO ₂	28
3.11 (a) (b) Dielectric constant and dielectric loss of material CCTO doped with 4% MnO ₂	29
3.12 (a) (b) Dielectric constant and dielectric loss of material CCTO doped with 5% MnO ₂	30
3.13 (a) (b) Temperature dependence of dielectric constant and dielectric loss of CCTO with different composition of MnO ₂ additive.....	31
4.1 Cole-Cole plot of pure CCTO at 27K, 49K and 141K Inset is the enlarged curves at low ϵ'' , ϵ'''	33
4.2 Arrhenius and Vogel-Fulcher Fitting of pure CCTO.....	36
4.3 (a) (b) Dielectric constant and loss of (1-y)CCTO + yCTO at 1 kHz.....	39
4.4 (a) (b) (c) XRD of pure CCTO and (1-y)CCTO + yCTO, y= 0.33, 0.89.....	40
4.5 Cole-Cole plot of (1-y) CaCu ₃ Ti ₄ O ₁₂ + y CaTiO ₃ , volume ratio y=0.5, 0.8 and 0.9	41
4.6 (a) Arrhenius and Vogel-Fulcher Fitting of 0.5 CCTO-0.5 CTO	43
4.6 (b) Arrhenius and Vogel-Fulcher Fitting of 0.2 CCTO-0.8 CTO.....	43
4.6 (c) Arrhenius and Vogel-Fulcher Fitting of 0.1 CCTO-0.9 CTO.....	44
4.7 Lichtenecker's Law Fitting to pure CCTO and CCTO-CTO.....	45

4.8 Cole-Cole plot of CCTO with 0.01 ~ 0.05 MnO ₂ additive at 180K.....	46
4.9 Multi Circle Fitting of CCTO with 0.01 MnO ₂ additive at 180K.....	48

CHAPTER I

INTRODUCTION

1.1 Background of $\text{CaCu}_3\text{Ti}_4\text{O}_{12}$

The dielectric properties of $\text{CaCu}_3\text{Ti}_4\text{O}_{12}$ material was first reported by Subramanian et.al in 2000.^[1] They first reported that large dielectric constants were found in $\text{ACu}_3\text{Ti}_4\text{O}_{12}$ (A= trivalent rare earth or Bi) type material. $\text{CaCu}_3\text{Ti}_4\text{O}_{12}$, displaying the most special behavior, shows a dielectric constant about 12,000 at 1 kHz, remaining steady in a large temperature range, from 100K to 400K . As we know, some materials with dielectric constants higher than 1,000 are associated with ferroelectric properties and the dielectric constant changes greatly during the ferroelectric phase transition. This property limits their applications in industry because often it is required that the dielectric constant of the material is fairly independent of the temperature. Therefore $\text{CaCu}_3\text{Ti}_4\text{O}_{12}$ (CCTO), with its low dependence on temperature, is of great interest to us.

Ferroelectric materials, like BaTiO_3 , always possess comparatively large dielectric constants due to ferroelectric phase transition and their perovskite structures. The dielectric response of BaTiO_3 mainly comes from the displacement of the Ti ions. With decreasing temperature, the Ti ion starts to displace from the centre, and the perovskite structure of BaTiO_3 changes from cubic to tetragonal at $\sim 130^\circ\text{C}$, then to orthorhombic at 0°C , and at last to rhombohedra at -90°C . However, in CCTO structure,

because the site symmetry of Ti is much less than that of BaTiO₃ structure, it is almost impossible for a ferroelectric phase transition to occur.

Shortly afterwards, other special features of CCTO were discovered by Ramirez et.al. [2] The crystal structure of CCTO is shown in Fig. 1.1. They reported that below 100 K the dielectric constant drops abruptly from around 12,000 to as low as 100, in addition to the fact that CCTO holds a large dielectric constant that barely varies in the temperature range from 100 K to 400 K as shown in Fig. 1.2(a). The reported dielectric loss, or $\tan\delta$ is less than 0.1 when the temperature is higher than 150 K, and a large peak occurs at around 100 K. Frequency dependence is also shown from 100 K to 300 K in a wide frequency range between 100 Hz to 1,000,000 Hz for both dielectric constant and

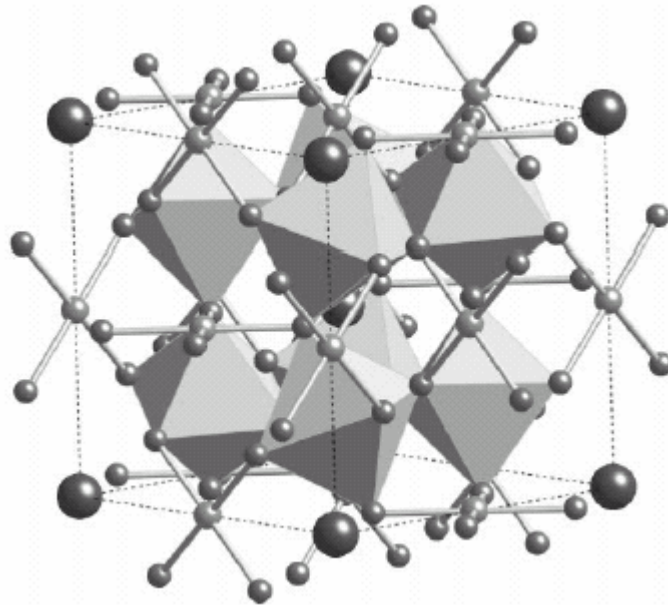


Figure 1.1 crystal structure of CCTO shown as TiO₆ octahedral, Cu atoms bonded to four oxygen atoms, and large Ca atoms without bonds [2]

loss. With the increasing frequency, the dielectric constant decreases in the entire temperature range and the dielectric loss peak shifts to higher temperature with small

increase in the maximum value of the peak. This behavior satisfies the relaxational excitation well.

Kolve and Bontchev also proved that the giant dielectric constant of CCTO doesn't come out of a classical ferroelectric phase transition by learning Raman spectroscopy of CCTO ^[3]. The large dielectric constants shown by many perovskite structure materials are caused by the atomic displacement within a non-centre symmetrical structure. However, after measuring the Raman spectra of CCTO micro-crystal in various scattering configurations, all the main Raman lines were able to be assigned to definite phonon modes in close comparison with results of lattice dynamical calculations, and no evidence for structural phase transition was found in the temperature range of 20 K to 600 K as shown in Fig. 1.3. Same results were given by neutron powder diffraction that CCTO structure remains cubic down to 35K. ^[4]

1.2 Impedance study and microstructure of $\text{CaCu}_3\text{Ti}_4\text{O}_{12}$

Therefore the origin of this giant dielectric constant and its weak temperature dependence becomes an interesting topic. Several different theories to explain this behavior have been proposed. One of the explanations raised in 2002 by Adams et al. was widely accepted ^[4]. This theory states that the dielectric behavior of CCTO does not come from its intrinsic character but from some heterogeneity of its ceramic structure.

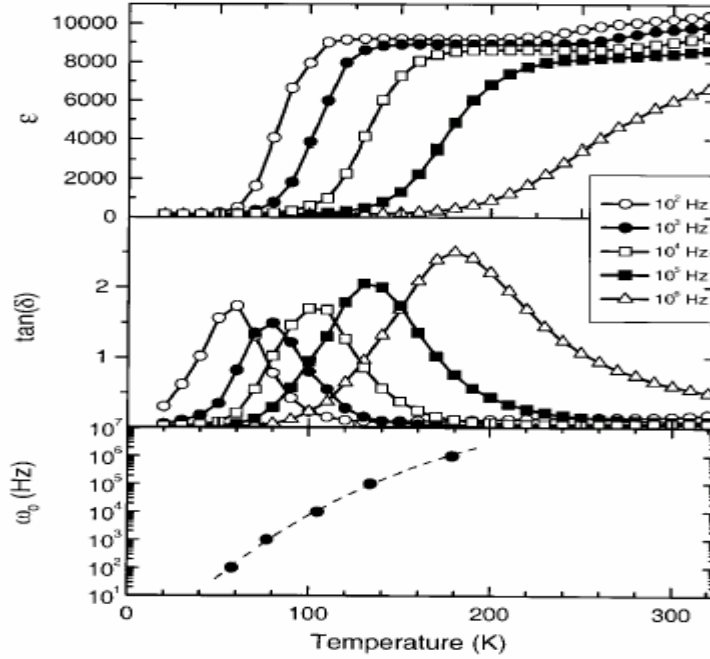


Figure 1.2 (a) Temperature-dependence of ϵ (a), $\tan\delta$ (b), and angular relaxation rate (c) at 10^2 , 10^3 , 10^4 , 10^5 and 10^6 Hz ^[2]

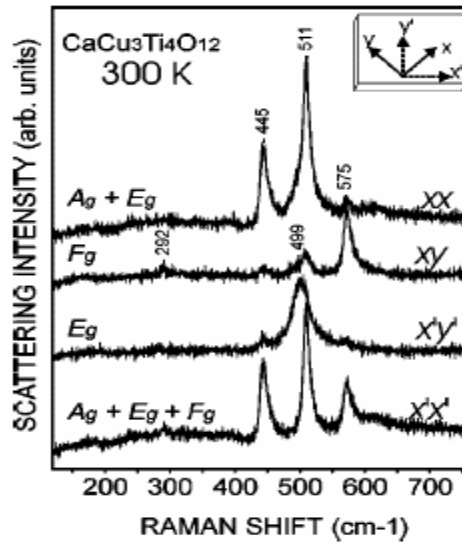


Figure 1.3 Polarized Raman spectra of CCTO at room temperature ^[3]

There is no structural phase transition in the whole temperature range, which is to say the permittivity doesn't come from the displacement of Ti ions, neither is it possible

that the dramatic decrease originates from the relaxation out of the samples. However, during the sintering step of any $ATiO_3$ - based samples (where $A= Ca, Sr, \text{ and } Ba$), they lose small amounts of oxygen and become conductive. Correspondingly, certain reoxidation creates insulating layers on the surface and along the internal boundaries of individual grains. This is called internal barrier layer capacitance (IBLC), which is considered to be the origin of the giant dielectric constant of CCTO.

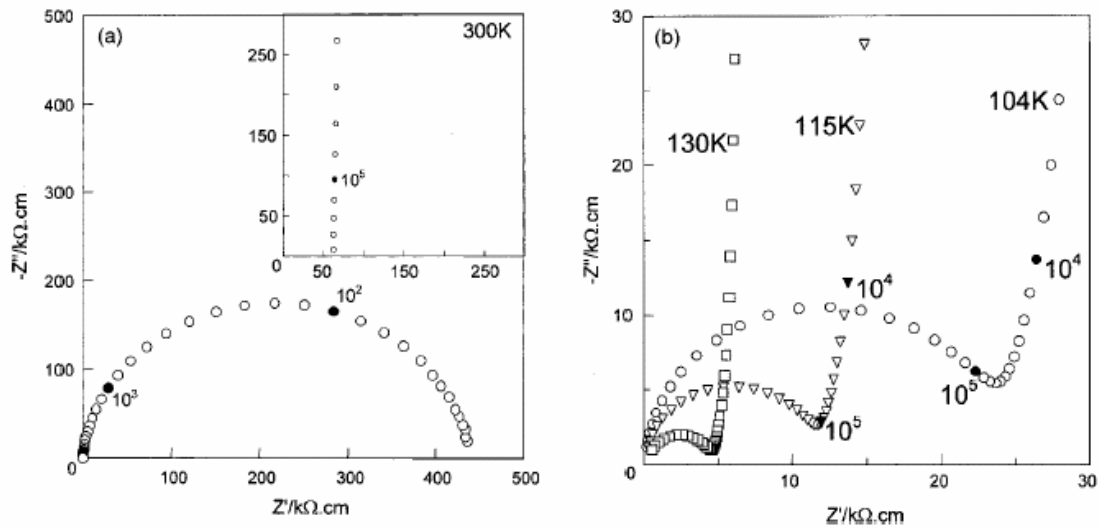


Figure 1.4 Complex impedance plot Z'' vs. Z' at (a) 300k and (b) 104,115 and 130k, for CCTO ceramics. The inset in (a) shows an expanded view of the high frequency data close to the origin. Filled symbols indicate selected frequencies in Hz ^[5]

Study of impedance spectroscopy proves that there exists no phase transition in CCTO material in detail. Experimental data, were simulated by an equivalent circuits, composed of two parallel RC elements connected in series, one representing semi-conducting grains and the other insulating internal layers. The grain and grain boundary responses can be identified by the impedance revealed in arcs. The plot for CCTO ceramics at room temperature (as shown in Fig. 1.4) has a large arc with nonzero intercept at high frequencies. It is shown that the first component has a resistance of 62

$\text{K}\Omega/\text{cm}$ with a comparatively lower capacitance. The second component, comparatively, has a resistance of $450 \text{ K}\Omega/\text{cm}$ and a much larger capacitance. Here the results are consistent and do not vary much with the sample. Therefore, this result indicates that CCTO ceramics consist of semiconducting grains and boundary layers regions with 10 times larger resistance. The origin of both the semiconductivity of the grains and the insulation is still to be discussed. The semiconductivity may possibly arise from the small loss of oxygen from the ceramics at high temperatures or from the intrinsic semiconductivity of the grains in case they are oxygen stoichiometric. The larger resistance of boundary layer, in the same way, is explained either by an intrinsic behavior of the boundary layers or by the oxygen-loss that induced insulating barriers in the ceramic. It is still unclear which one of the two interpretations is correct so far.

The scanning electron Microscopic (SEM) graphs of CCTO ceramics were reported when sintered at 1100°C for (a) 3 hours and (b) 24 hours. An interesting difference was found. Firstly, it is obviously that the grain size increases from an average of less than $10\mu\text{m}$ to around $300\mu\text{m}$, which is more than 30 times larger. Secondly, the impedance measurement at 1 KHz shows great enhancement of dielectric constant from $\sim 9,000$ of 3h to $\sim 280,000$ of 24h. Also the conductance measurement shows that the resistivity goes down from $4.2 \text{ M}\Omega\text{cm}$ to $0.18 \text{ M}\Omega\text{cm}$. These facts are obviously associated. It is clear that with increasing grain size which is also a decrease in the total

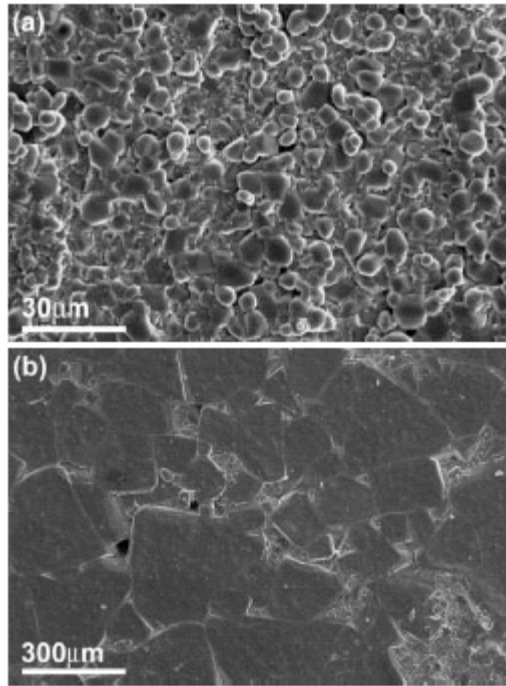


Figure 1.5 SEM images of ceramic microstructure for CCTO ceramics sintered at 1100C for a) 3h and b) 24h ^[6]

volume fraction of boundary layer, the overall permittivity decreases because the total number of capacitors that constructed by these micro layers increases, while total conductivity decreases as parts of the insulating boundary layer vanish.

1.3 Doping methods

Two main features are needed for any dielectric material in practical applications: high dielectric constant and low dielectric loss. CCTO exhibits a very high value of dielectric constant, which has been found to be ~100,000 over a wide temperature range.

^[2] However, the dissipation factor (which is also referred to as the loss tangent $\tan \delta = \epsilon''/\epsilon'$, where the angle δ is supplementary angle of the phase difference between the applied electric field and the induced current) of pure CCTO is relatively too high. The value of loss tangent has been found to be about 0.115 at 1 MHz at room temperature. ^[6]

Therefore CCTO, although it presents a large dielectric constant, fails to meet the second requirement. To reduce the dissipation factor while keeping the dielectric constant, different methods were proposed to solve this problem, such as applying different sintering methods or doping additional oxides.

In Patterson et al.'s work ^[7], the effects of the isovalent dopant ZrO₂ on the dielectric properties of CCTO were investigated. Different percentages (0.1 %, 0.5 % and 1.0 wt %) of ZrO₂ powders were added to CCTO. It was found that 0.5 wt % ZrO₂ doped CCTO exhibits a permittivity over 4900 and a dielectric loss below 5 % over a wide frequency range from 50 Hz to 30 KHz at room temperature. X-ray diffraction (XRD) was utilized in their work to observe changes in lattice parameters and phase evolution. The XRD data showed a modest decrease in lattice parameters with the addition of dopant up to 0.5 wt %, while there was no noticeable change in lattice parameter with higher concentration of ZrO₂. Therefore it was concluded that the added ZrO₂ was most likely present in the microstructure either in the grain boundaries or as a second phase. The XRD data also showed that there was no second phase and the grain size that remained constant at the value of approximately 5 μm independent of the dopant concentration. So it was concluded that ZrO₂ doping increased the resistivity of boundary layers and therefore decreased dielectric loss dramatically.

Similar doping methods were also investigated. The La for Ca substitution was recently reported by Feng et al. ^[8]. The results showed that the dielectric loss was greatly decreased while dielectric constant remains high, as 20% La substitution reduced the tan δ value to 0.015 for 10 KHz from 180K to 300K. Based on IBLC theory, the dissipation induced by the resistance of the semi-conducting grains affects greatly

dielectric loss. La doping strongly reduced the resistance in the grains so that it suppressed the dielectric loss.

Co, Ni, and Fe doping was studied by Chiodelli et al.^[9] Dielectric constant of CCTO was dramatically increased by such doping, shown as Table 1.1.

Especially in the case of 5% Co doping, the dielectric constant was raised to 150,000, which is 50 times larger than that of CCTO.

Table 1.1 Effects of Co, Ni, Fe doping in CCTO Material

Sample	AC capacitance (nF)	DC capacitance (nF)	DC R (Ω)
Co 5%	47	> 25	$\sim 1 \times 10^6$
Ni 5%	34	> 20	$\sim 2 \times 10^5$
Co 2%	20	> 10	$\sim 1 \times 10^6$
Fe 2%	10	> 10	$\sim 2 \times 10^8$
Pure	1.1	> 1	$\sim 4 \times 10^8$

Doping method opens an effective way to alter the electric performance, as mentioned above, both high ϵ and low $\tan\delta$ are essential for capacitance application. However, in the current literature, less attention was given to the lowering of the dielectric loss ($\tan\delta$). A high loss greatly blocks its use in electronic industry. Further work on lowering the loss while remaining the high dielectric constant becomes desirable. In this work, CaTiO_3 and MnO_2 were doped to improve the performance of material $\text{CaCu}_3\text{Ti}_4\text{O}_{12}$. The performances of these materials were studied.

CHAPTER II

EXPERIMENTAL PROCEDURE

Four sets of samples: $\text{CaCu}_3\text{Ti}_4\text{O}_{12}$, $\text{Ca}_2\text{Cu}_2\text{Ti}_4\text{O}_{12}$ and $\text{Ca}_3\text{CuTi}_4\text{O}_{12}$ for X-ray Diffraction examination, $(1-y)\text{CaCu}_3\text{Ti}_4\text{O}_{12} + y\text{CaTiO}_3$ ($y=0.5, 0.8$ and 0.9) and $\text{CaCu}_3\text{Ti}_4\text{O}_{12} + \delta\text{MnO}_2$ ($0.01 \leq \delta \leq 0.05$) have been prepared by solid state reaction in this work. The experimental procedure includes 1.sample preparation, 2.structure and density examination, 3.dielectric and electrical properties measurements.

2.1 Sample Preparation

2.1.1 Compositions

Samples were prepared from well ground mixtures of raw materials CaCO_3 , CuO , TiO_2 , and MnO_2 , according to the composition. The starting raw materials were of high purity (as shown in Table 2.1).

Table 2.1 Purity level of the raw reagents

Reagents	CaCO_3	TiO_2	CuO	MnO_2
Purity	>99.9%	>99.9%	>99.99%	>99.99%

(1) Pure $\text{CaCu}_3\text{Ti}_4\text{O}_{12}$

Pure CCTO was made as following solid state reaction:



(2) $\text{CaCu}_3\text{Ti}_4\text{O}_{12}$ incorporating with CaTiO_3

Considering the composition of $(1-y) \text{CaCu}_3\text{Ti}_4\text{O}_{12} + y \text{CaTiO}_3$, where y is the volume ratio ($y=0.5, 0.8$ and 0.9), samples with 3 different compositions were made.

$\text{Ca}_2\text{Cu}_2\text{Ti}_4\text{O}_{12}$ and $\text{Ca}_3\text{CuTi}_4\text{O}_{12}$ were prepared as well.

(3) $\text{CaCu}_3\text{Ti}_4\text{O}_{12}$ doped with MnO_2

For the samples $\text{CaCu}_3\text{Ti}_4\text{O}_{12} + \delta \text{MnO}_2$, 5 different compositions ($\delta = 0.01, 0.02, 0.03, 0.04, 0.05$) were prepared.

2.1.2 Weighing and mixing

The raw powder materials were weighed using an electric balance with an accuracy of 0.0001 gram. Reagents were mixed in an agate mortar with alcohol, and then set in a planetary mill with 30 rounds per minute for 4 hours to be sufficiently mixed. Powders were dried in an oven at 80°C to vaporize alcohol, and were sieved with a 0.45mm sieve to avoid agglomerations.

2.1.3 Calcining

The mixed powders were poured in a crucible and then calcined in an electrical temperature-controlled furnace, strictly following such 3 steps:

Step 1: Starting from room temperature, raise to 500°C in 3 hours evenly, keep constant at 500°C for 2 hours;

Step 2: then raise to 850°C in 2 hours evenly. Keep constant at 850°C for one hour ;

Step 3: at last raise to 1100°C from 850°C in 2 hours evenly, keep constant at 1100°C for 2 hours.

The reason for keeping temperatures constant for a few hours at 500°C , 850°C is so that any water and alcohol that may still exist in the material will vaporize at these 2

temperatures, while 1100 °C is the definite temperature at which the solid state reaction starts.

2.1.4 Pressing

The calcined powders were firstly milled and then sieved using a 0.35mm sieve before pressing. They were pressed into pellets of diameter ~ 5mm and thickness of 0.5 to 1.5 mm under a pressure of 300MPa. Pressure was carefully chosen as powders would not stick if it is too low and inner structure would break if too high. In the case of incorporating with CaTiO₃, a small amount of binder was used to help the pellets hold their shape.

2.1.5 Sintering

The pellets were then put in a high-temperature furnace to be sintered, with the increases in temperature following these 3 steps; first two steps are exactly the same with the Calcining part:

Step 3: Raise to 1250 °C from 850 °C in 3 hours evenly, and then keep constant at 1250 °C for 2 hours.

Notice that due to different solid state reaction temperatures of CaTiO₃ and CCTO, the highest sintering temperature varies from 1150 °C to 1250 °C, respectively.

2.2 Structure and density examination

2.2.1 Density Measurement

The sintered pellet samples were first polished into a smooth cylinder. Thickness and diameter were then measured using a venier caliper with an accuracy of 0.05mm. Density obtained based on these measurements will be used when comparing with the theoretical density.

2.2.2 X-ray Diffraction examination

Sintered samples were ground into powders with an agate pestle and mortar to fit the requirement for the X-ray diffraction measurements. The power X-ray diffraction measurement was carried out with a PW1710 BASED Diffractometer. The tube anode was Copper. And the parameters are listed in Table 2.2.

Table 2.2 Parameters used in X-ray diffraction measurement

Diffractometer type	PW1710 BASED
Tube anode	Cu
Generator tension [kV]	40
Generator current [mA]	35
Wavelength Alpha1	1.54056
Wavelength Alpha2	1.54439
Intensity ratio (alpha2/alpha1)	0.500
Divergence slit	AUTOMATIC
Irradiated length [mm]	12
Receiving slit	0.2
Monochromator used	YES

In the measurement the sample was scanned continuously. The starting angle was 2, ending angle was 59.990, step size was 0.020 and time per step was 1.000 s.

2.3 Dielectric and electrical properties measurements

2.3.1 Dielectric properties measurements

Silver electrodes were sputtered on both the top and bottom of the cylinder shaped samples for 4 minutes each, using Edwards Coating System sputter coater. Cables were then connected to both sides. Now a parallel plate capacitor has been made and is ready to be measured.

A cryostat system (ARS Inc M/N ARS-2 W water cooler and ALCTEC Vacuum Cryostat) was employed for dielectric and electrical measurement. Firstly, the sample is

mounted into a copper cylinder in the container, since copper is a good conductor of heat and the experiment is extremely temperature sensitive. A small piece of quartz is mounted between the sample and the support as well to avoid contacting between each other (which may cause serious damage to the equipment). This whole set is placed in a well-sealed chamber of the cryostat which will be pumped to high vacuum before changing the temperature. Also two temperature sensors are placed in the chamber, one right next to the sample and the other next to the heater.

Dielectric measurements were carried out by a Solartron SI1260 Impedance / gain-phase analyzer and a Solartron 1296 Dielectric Interface. The temperature was controlled by a Lakeshore 331 Temperature Controller. First the temperature is increased to 430K and then begins to decrease, measurements are taken every 5K to as low as 7K. At every single temperature point there is a 2 minute idling time before measurements to begin allowing the temperature grads to stabilize. 0.1Hz to 1MHz was the frequency range and 40 frequencies were arranged uniformly in a logarithm scale. The experimental data including dielectric constant, dielectric loss, etc. was then automatically recorded by the computer in the time order with the aid of Solartron SMaRT analytical software.

2.3.2 Electrical properties measurements

Since CCTO is semiconductor, there exists a giant contact resistor between the material and the silver electrode. Generally, 2-probe electrode method cannot eliminate the contact resistor because only 1 voltage and 1 current could be obtained, which gives a result containing contact resistor. 4-probe electrode, comparatively, measures another group of voltage and current in the mean time, which excludes the contact resistor and gives a more accurate result. Therefore, the 4-probe electrode method was used to carry

out the measurement in our study. (Electrodes that connected to the sample are shown in Fig. 2.1) The experiment was performed in the temperature range from 430K to 10K, and data was collected every 5K.



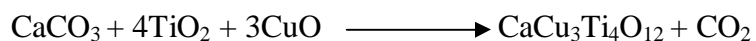
Figure 2.1 The dark parts are covered with electrodes and are each connected to a cable

CHAPTER III

EXPERIMENTAL RESULTS

3.1 Pure CaCu₃Ti₄O₁₂ ceramics

CaCu₃Ti₄O₁₂ (denoted as CCTO) is formed via the following solid state reaction:



Samples were pressed into pellets in a cylinder shape. After sintering, the pellets were polished. The thickness, diameter and weight of the pellets were then measured. The densities of the samples could therefore be calculated using the following equation,

$$r = \frac{m}{p \cdot (D/2)^2 \cdot t}, \text{ where } r, m, D, t \text{ stand for density, mass, diameter and thickness,}$$

respectively. The measured density is shown in Table 3.1.

Table 3.1 Density measurements of CCTO samples

	Diameter (<i>D</i>)		Thickness (<i>t</i>)		Weight (<i>m</i>) (g)	Density (<i>r</i>) (g/cm ³)
	(inch)	(mm)	(inch)	(mm)		
Sample 1	5.32	13.51	0.55	1.41	1.000	4.95
Sample 2	5.31	13.49	0.56	1.42	1.014	4.92

For both samples similar density was obtained, the average of which is around 4.93 g/cm³ from the calculations. The theoretical density calculated from lattice

parameters is 5.09g/cm^3 . The relative density $\rho/\rho_{\text{theoretical}} = 97\%$, indicating that dense CCTO ceramic samples were obtained.

The temperature dependence of the dielectric constant (ϵ) and the dielectric loss ($\tan\delta$) for pure $\text{CaCu}_3\text{Ti}_4\text{O}_{12}$ sample in a frequency range of 0.1Hz to 1MHz from 20K to 420K are shown in Fig.3.1 (a) (b).

In Fig. 3.1 (a), the dielectric constant (ϵ) at room temperature is 18,400 at 1 kHz, which is in accordance with the results of Subramanian et al. [1]. The dielectric constant drops as temperature decreases. General dielectric relaxation theory applies in this case: the lower the frequency, the higher its dielectric constant. Over the temperature range from 100K to 330 K, dielectric constant is extremely large and weakly dependent on temperature.

On cooling below 100 K, however, it drops sharply by a factor of 100 to as low as 150 at 1 kHz and forms a shoulder shape in this range. This shoulder shifts to higher temperature with increasing frequency while its height barely changes.

Fig. 3.1(b) shows that a set of loss peaks occurs in the temperature range of 20K to 200K where the ϵ shoulder is present as shown in Fig.3.1 (a). The peaks are shifted to higher temperatures with increasing frequency and their intensity increases simultaneously.

Above 200K, the dielectric loss ($\tan\delta$) increases significantly with temperature at low frequencies. It is seen that both the dielectric constant and loss vary greatly with different frequencies in the measured temperature range. This frequency dispersion indicates the existence of relaxation behavior for pure CCTO.

It's interesting to note that an extra set of $\tan\delta$ peaks around 150K ~ 350K is revealed from 10 to 1000 Hz as shown in Fig 3.1 (a).

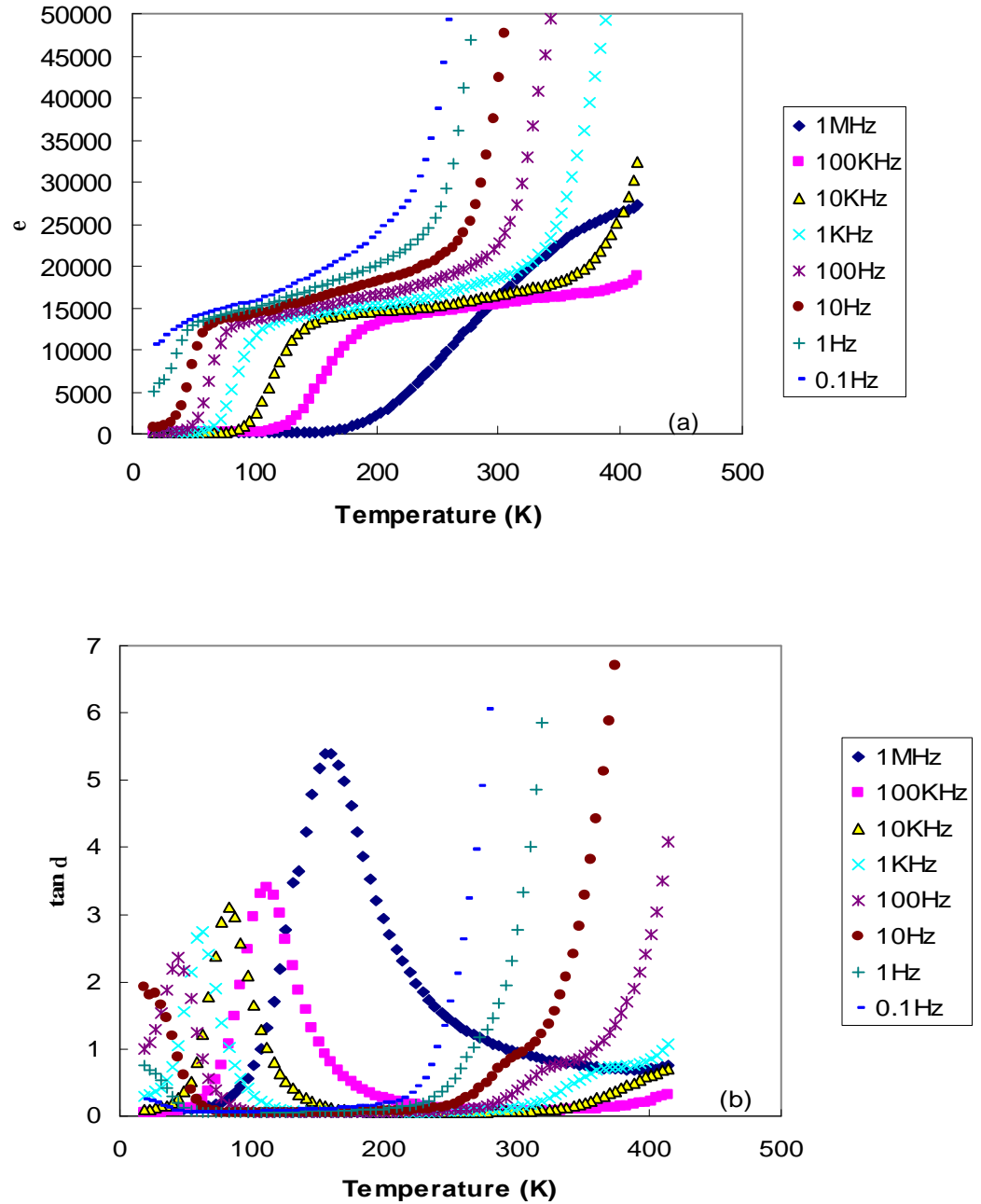


Figure 3.1(a), (b) Dielectric constant (ϵ') and dielectric loss ($\tan\delta$) of pure CCTO

In order to compare the behavior between the dielectric constant and dielectric loss at different frequencies, both ϵ and $\tan\delta$ are replotted from 20K to 430K at 1 kHz and 100 kHz in Fig. 3.2.

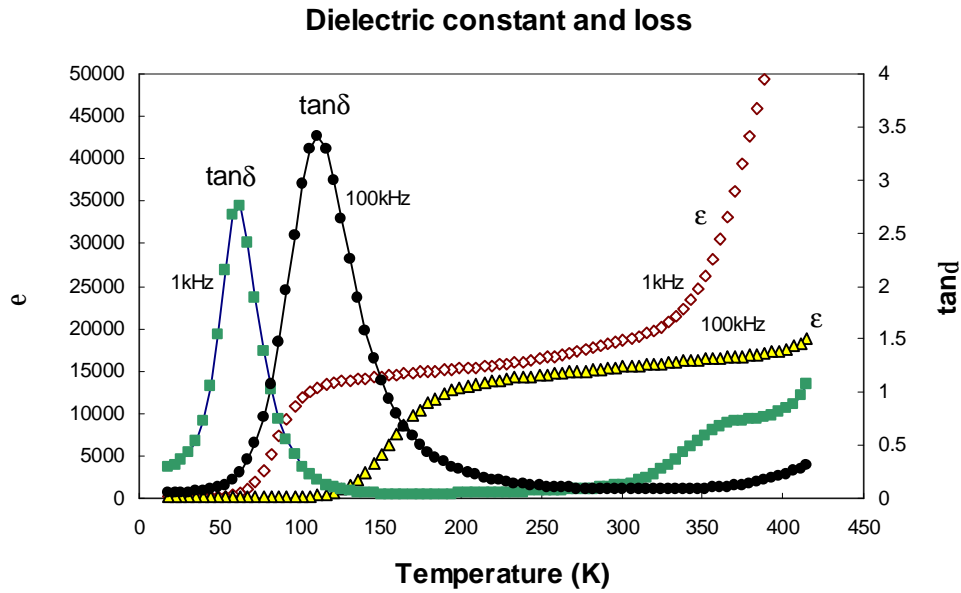


Figure 3.2 Dielectric constant and loss vs. temperature

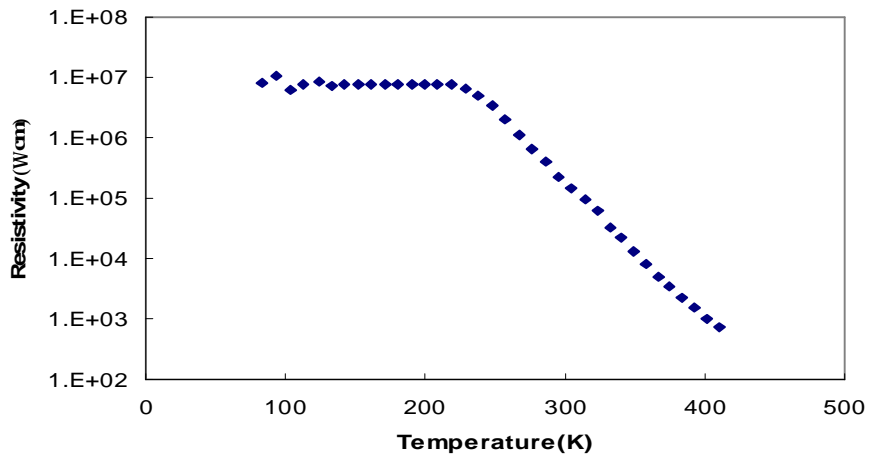


Figure 3.3 Resistivity vs. Temperature

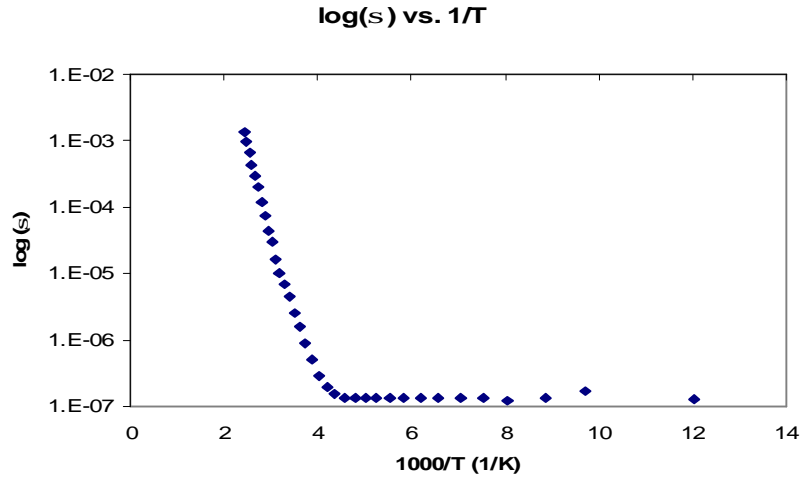


Figure 3.4 Conductivity vs. 1/T

In Fig. 3.2, the sharp peak in dielectric loss ($\tan \delta$) shows up at around 100K for 100 kHz, and corresponds to the temperature where dielectric constant starts to increase with increasing temperature.

The conducting behavior of pure $\text{CaCu}_3\text{Ti}_4\text{O}_{12}$ sample is also studied. The resistance vs. temperature is shown in Fig. 3.3 and conductivity (σ) vs. reciprocal temperature ($1/T$) is plotted in Fig. 3.4. With decreasing temperature, the resistance first increases linearly from $900 \Omega\text{cm}$ to $10^7 \Omega\text{cm}$ from 420K to 230K, then remains at a constant of $10^7 \Omega\text{cm}$ from 230K until as low as 20K. Correspondingly, there are two slopes in σ vs. $1/T$ plot, implying a complicated conduction mechanism.

3.2 (1-y) $\text{CaCu}_3\text{Ti}_4\text{O}_{12}$ + y CaTiO_3 (volume ratio y=0.5, 0.8 and 0.9)

(1-y) $\text{CaCu}_3\text{Ti}_4\text{O}_{12}$ + y CaTiO_3 is studied, where y is the volume ratio (y=0.5, 0.8 and 0.9). Samples of three different compositions were prepared and examined. The temperature dependence of the dielectric constant (ϵ) and dielectric loss ($\tan\delta$) are plotted and shown in Fig. 3.5 to Fig. 3.7

The behaviors of CCTO incorporating with CTO are similar to those of CCTO: 1. There exists a shoulder like behavior in ϵ , corresponding to a $\tan\delta$ peak below 200K; 2. Obvious frequency dispersion is seen in the whole temperature range; 3. Both ϵ and $\tan\delta$ increase drastically at higher temperatures. However, for CCTO-CTO ceramics, both ϵ and $\tan\delta$ are greatly suppressed. From Fig. 3.5 (a) to Fig.3.7 (a), with increasing concentration of CaTiO_3 , the dielectric constant at 200K decreases gradually from 15,000 to 800 for 1 kHz; the peak of dielectric loss drops from 5.9 to 0.22 as well.

The dielectric constants, the temperature where the loss peak occurs, and $\tan\delta$ maximum of CCTO-CTO samples are summarized in Table 3.2.

Table 3.2 Dielectric properties of (1-y) CCTO – y CTO

	ϵ at 200K for 1kHz	$\tan\delta$ at 1kHz	
		T_m	$\tan\delta$ maximum
Pure CCTO	15286	62.3K	2.72
0.5 CCTO + 0.5 CTO	3831	125K	0.70
0.2 CCTO + 0.8 CTO	1695	121K	0.522
0.1 CCTO + 0.9 CTO	381	206K	0.224

In Fig. 3.6 (a) and Fig. 3.7 (a), the profiles of those two shoulders look different. The dielectric constant ϵ in Fig. 5 (a) increases much more quickly than it does in Fig. 6 (a), and presents a flatter plateau region from 100K to 330K; as to ϵ in Fig. 6 (a), comparatively, the curve becomes smoother in the whole temperature range.

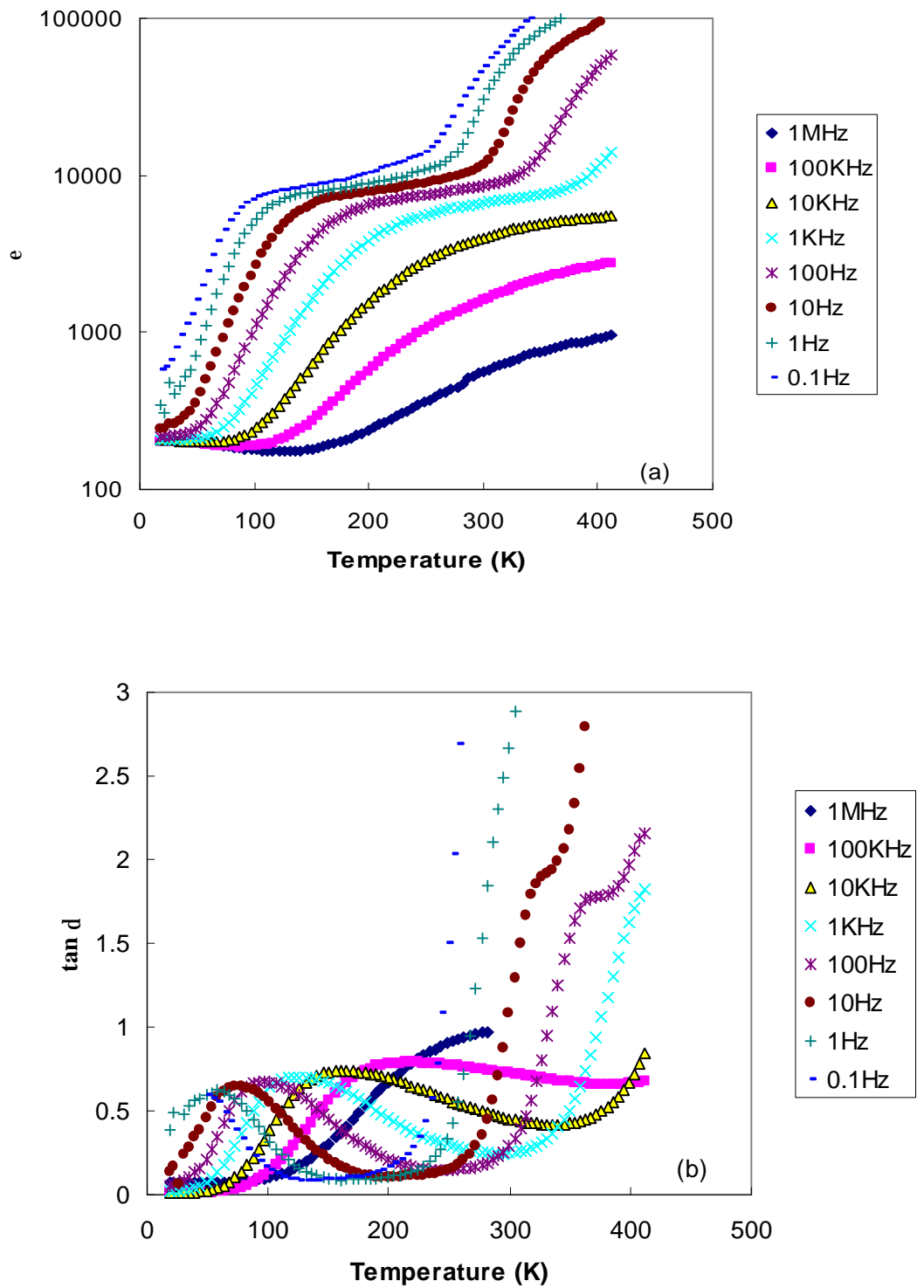


Figure 3.5 (a) (b) Dielectric constant (ϵ) and dielectric loss ($\tan\delta$) of material 0.5CCTO+0.5CTO

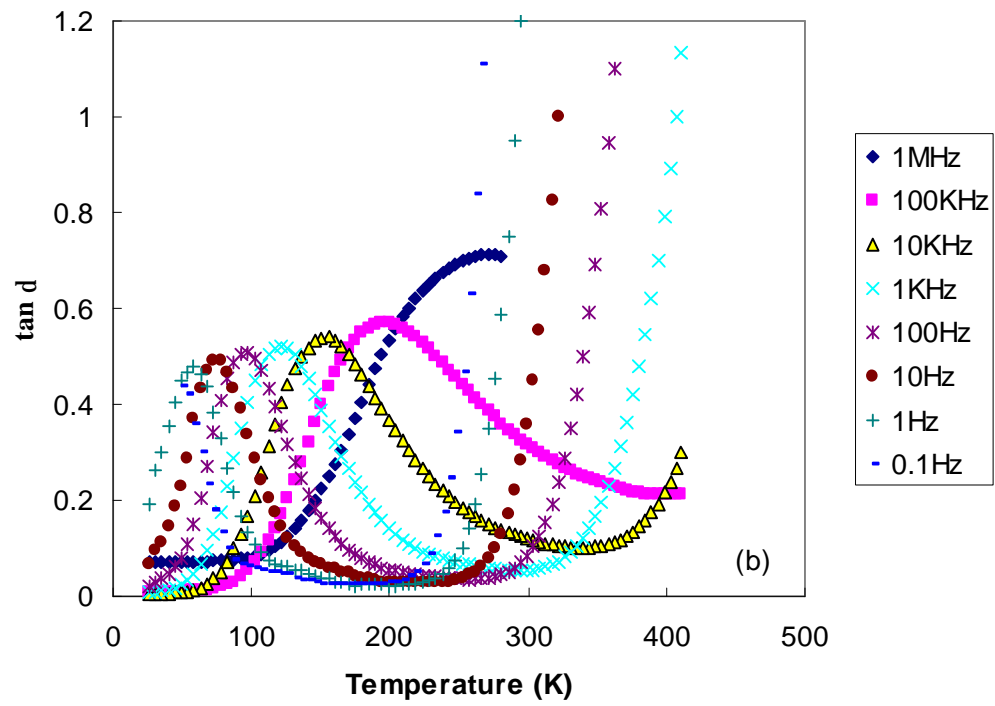
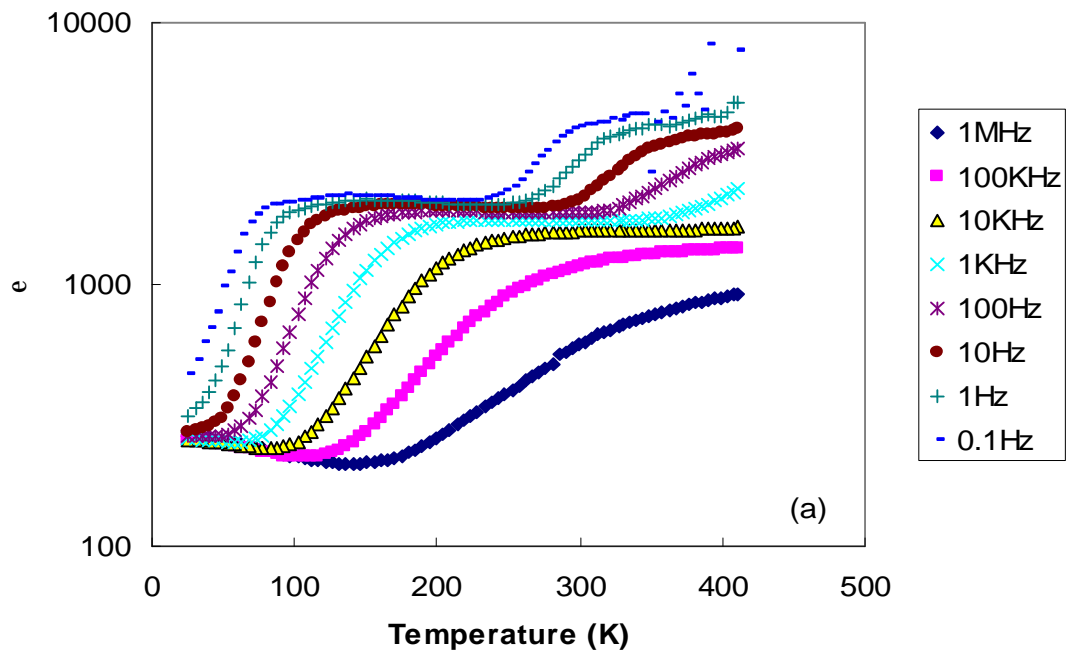


Figure 3.6 (a) (b) Dielectric constant (ϵ) and dielectric loss ($\tan\delta$) of material 0.2CCTO + 0.8CTO

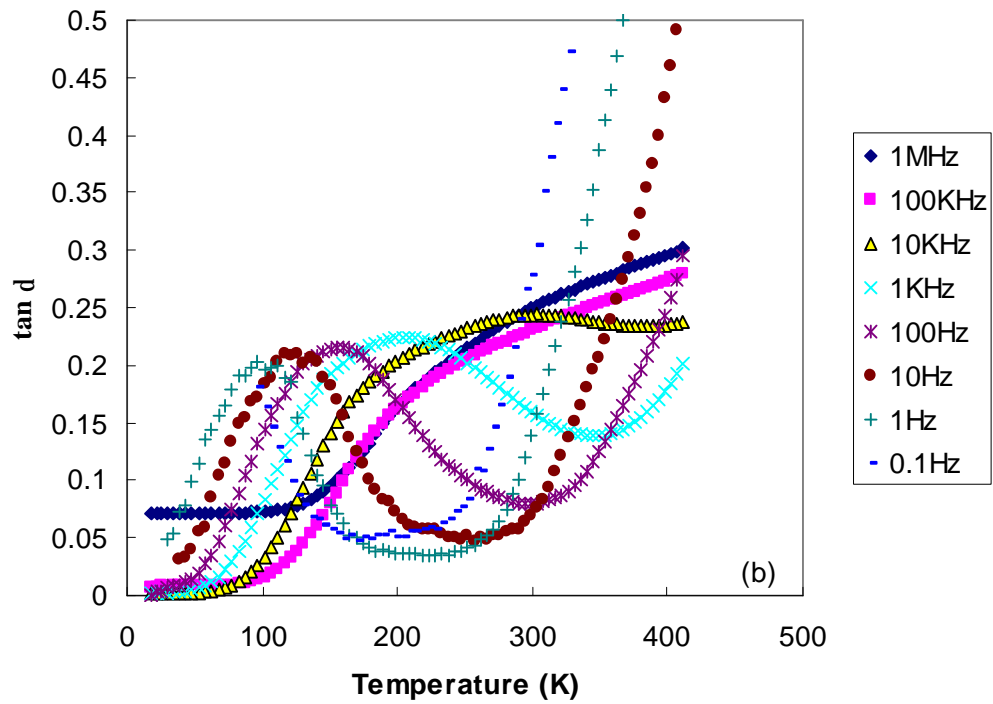
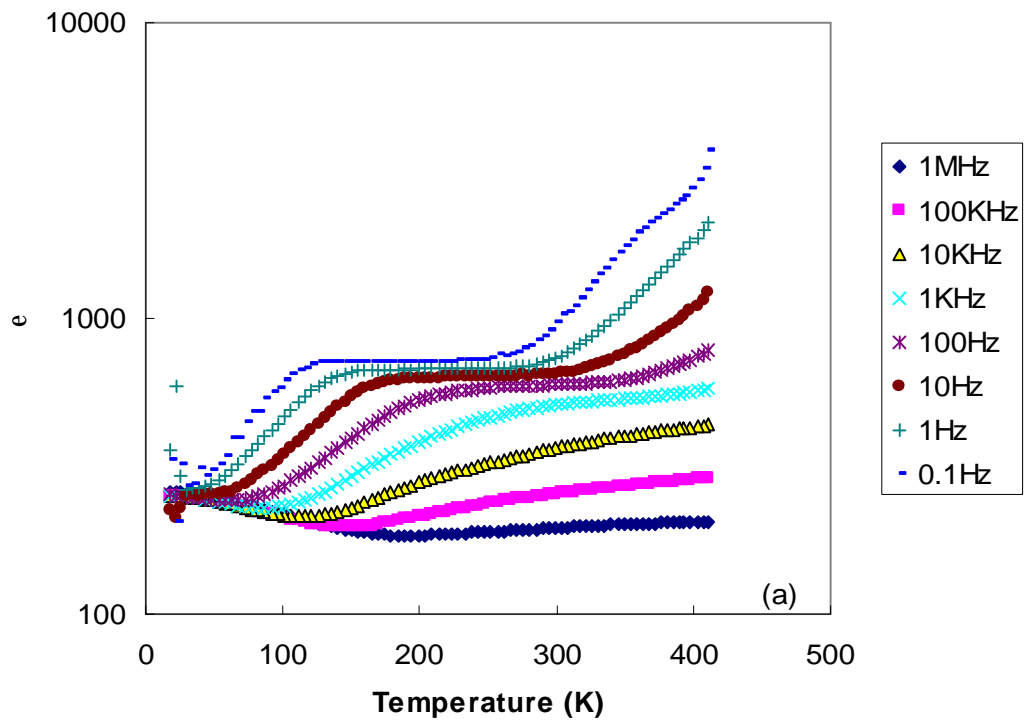


Figure 3.7 (a) (b) Dielectric constant (ϵ) and dielectric loss ($\tan \delta$) of material 0.1 CCTO + 0.9CTO

The second set of $\tan\delta$ peaks shown in the range of 250K to 430K is well presented in Figs. 5 (b), 6 (b) and 7(b). It can be seen that there are two separate $\tan\delta$ peaks in these plots; one group is from 50K to 250K and the other from 250K to 430K. With increasing CaTiO_3 amount, the first set of peaks still exists but is suppressed to some extent, while the second set of peaks completely vanishes.

3.3 CCTO doped with MnO_2

Five different compositions of $\text{CCTO} + \delta\text{MnO}_2$ ($\delta = 0.01, 0.02, 0.03, 0.04$ and 0.05) samples were prepared and examined. The temperature dependence of the dielectric constants and dielectric loss was plotted and is shown below:

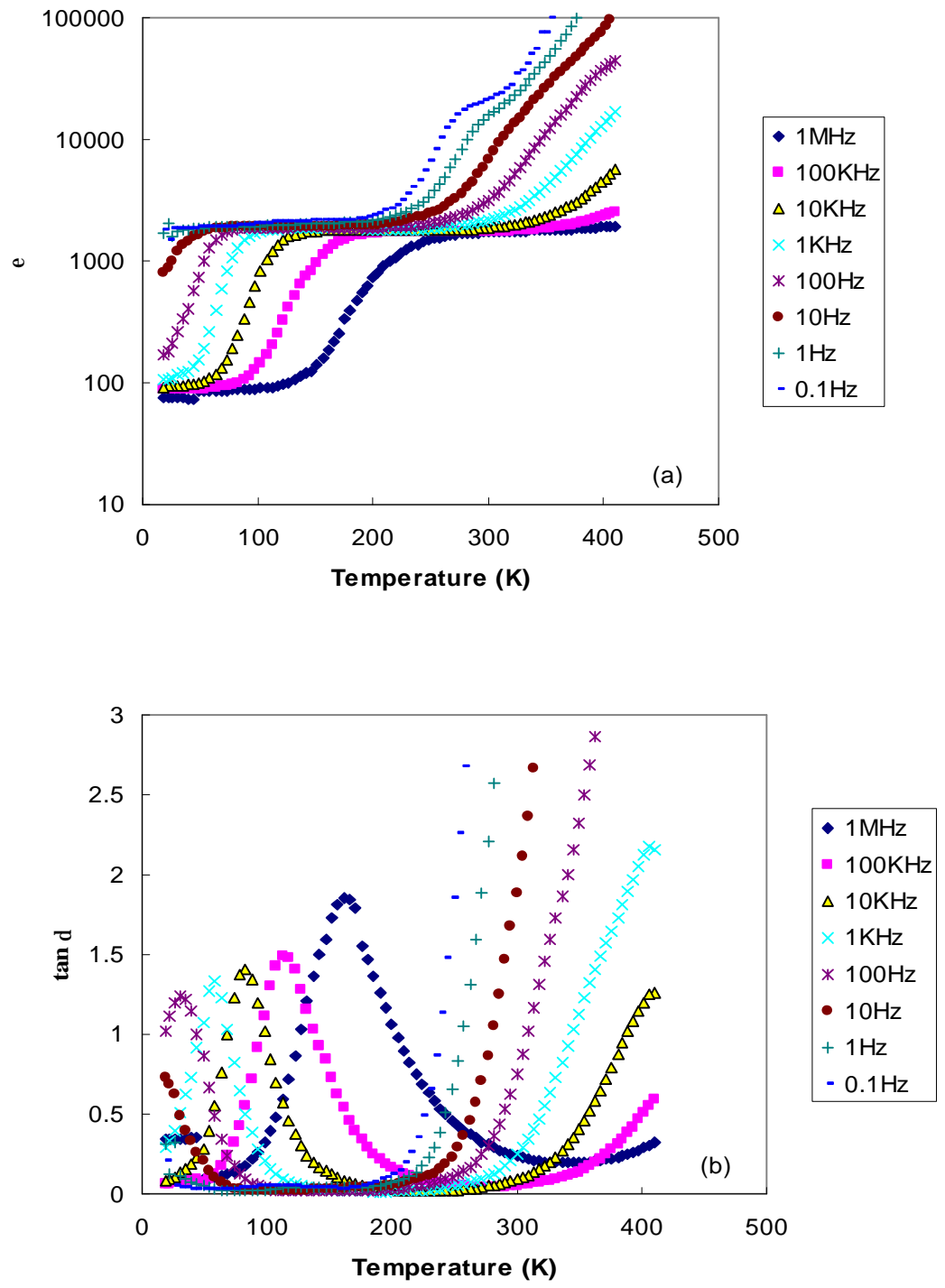


Figure 3.8 (a) (b) Dielectric constant (ϵ) and dielectric loss ($\tan \delta$) of material CCTO doped with 1% MnO₂

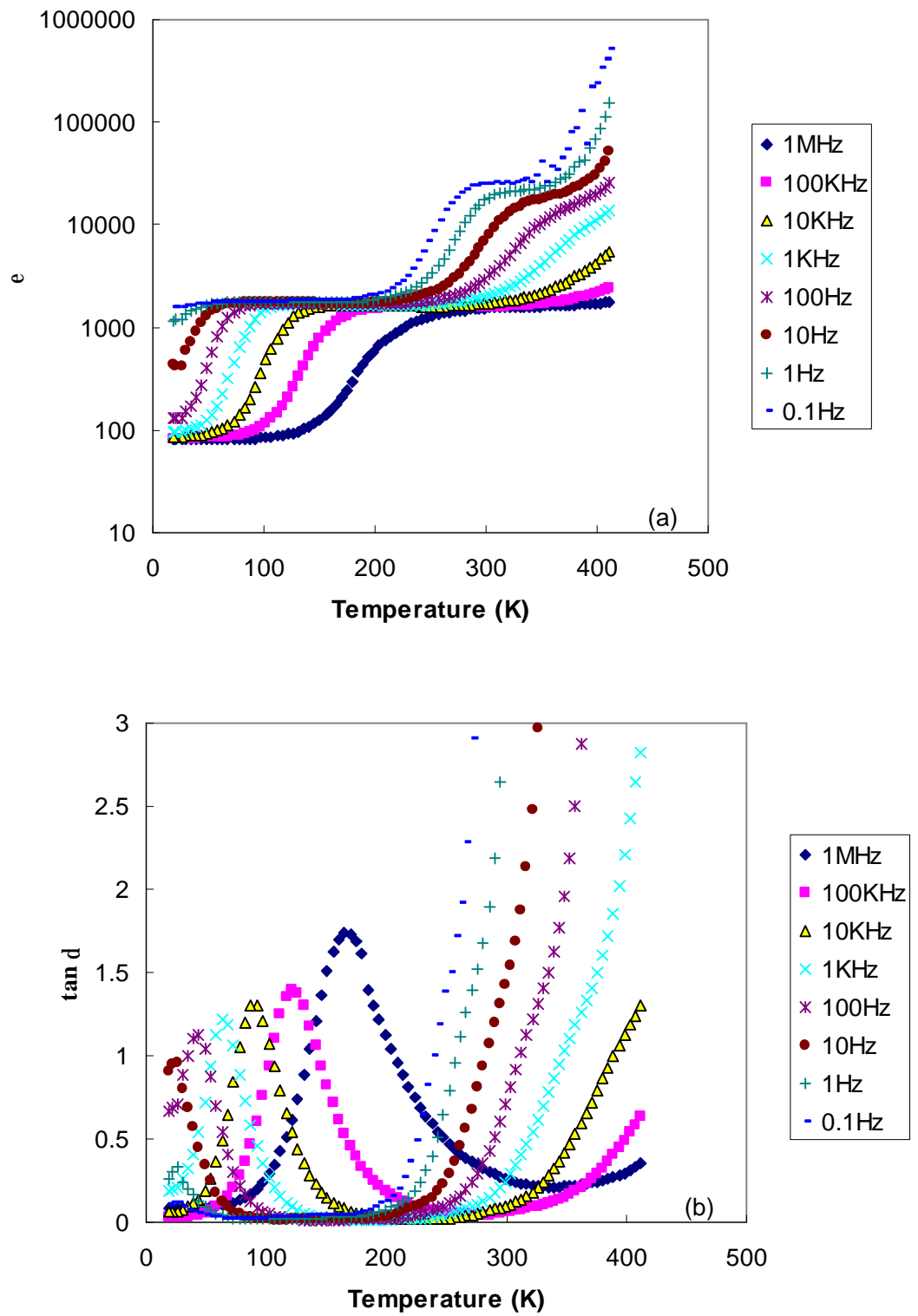


Figure 3.9 (a) (b) Dielectric constant (ϵ) and dielectric loss ($\tan \delta$) of material CCTO doped with 2% MnO₂

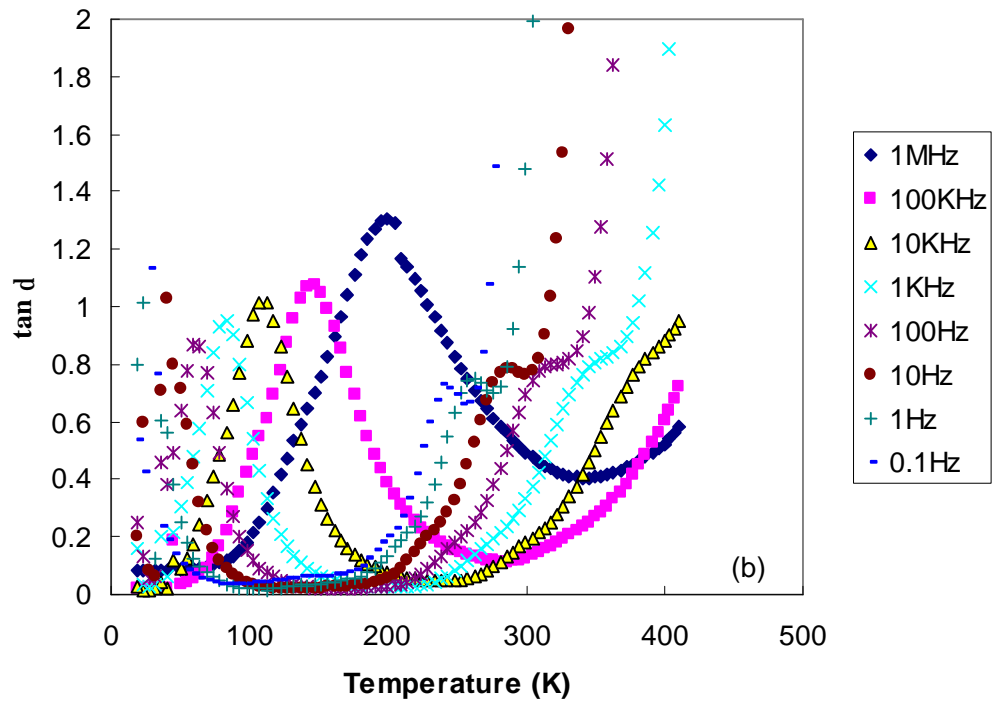
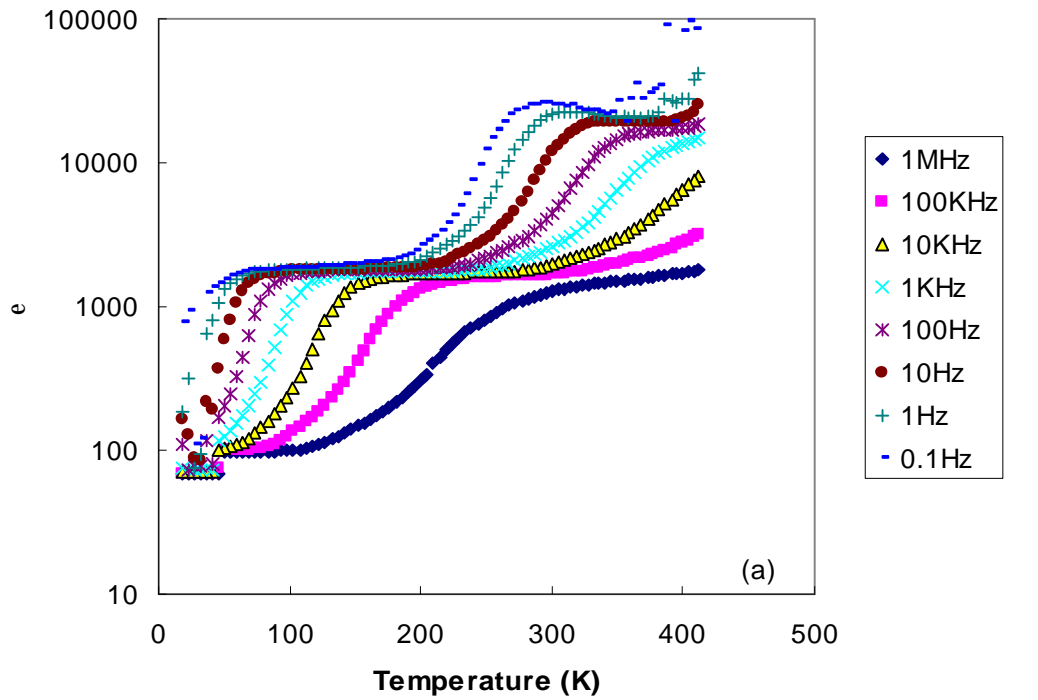


Figure 3.10 (a) (b) Dielectric constant (ϵ) and dielectric loss ($\tan\delta$) of material CCTO doped with 3% MnO_2

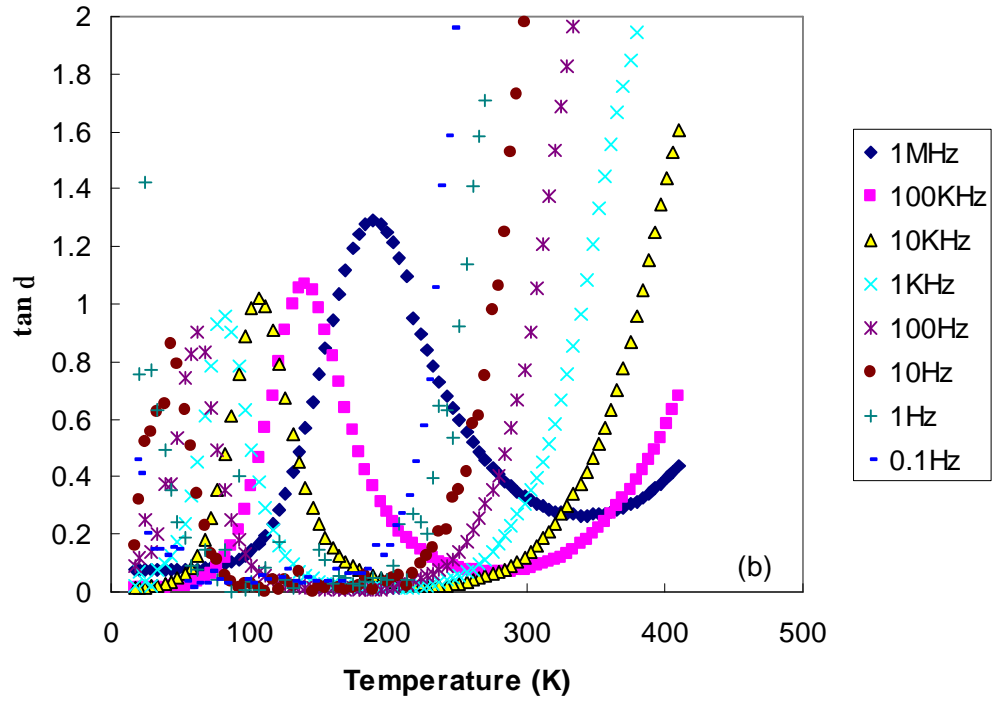
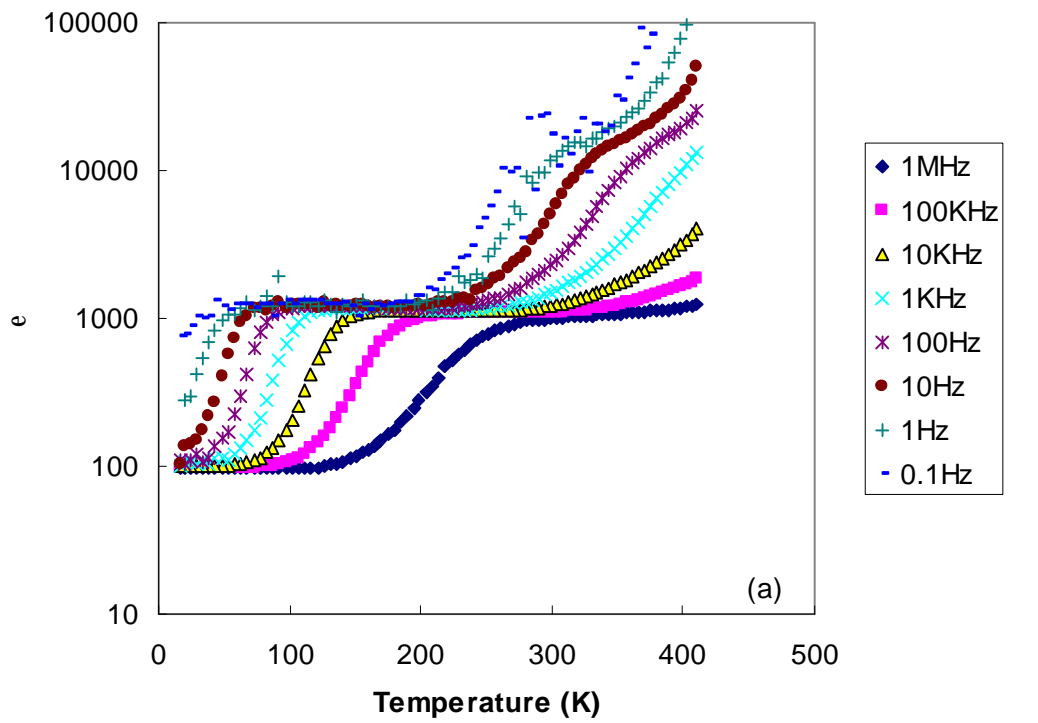


Figure 3.11 (a) (b) Dielectric constant (ϵ) and dielectric loss ($\tan \delta$) of material CCTO doped with 4% MnO_2

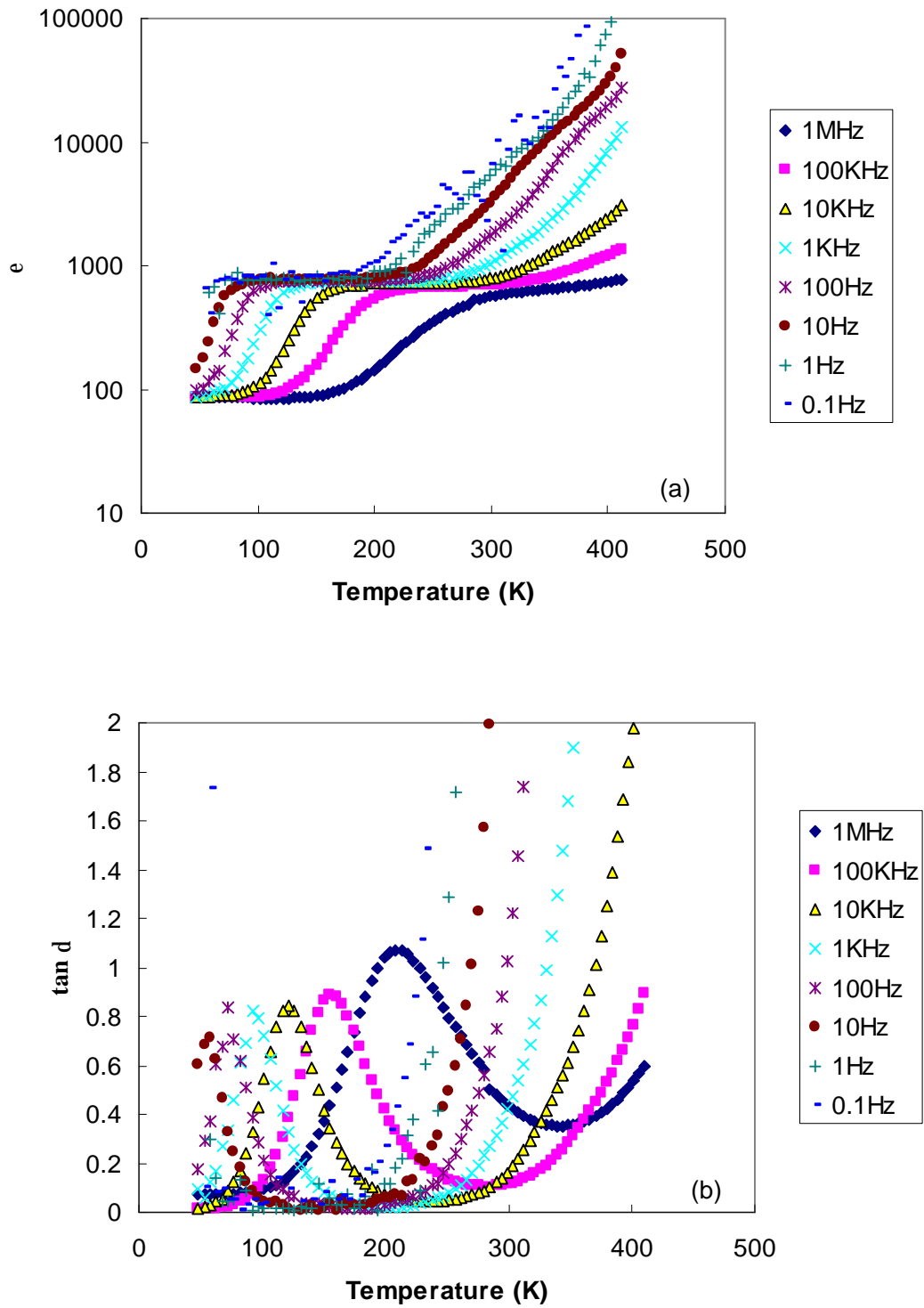


Figure 3.12 (a) (b) Dielectric constant (ϵ) and dielectric loss ($\tan \delta$) of material CCTO doped with 5% MnO₂

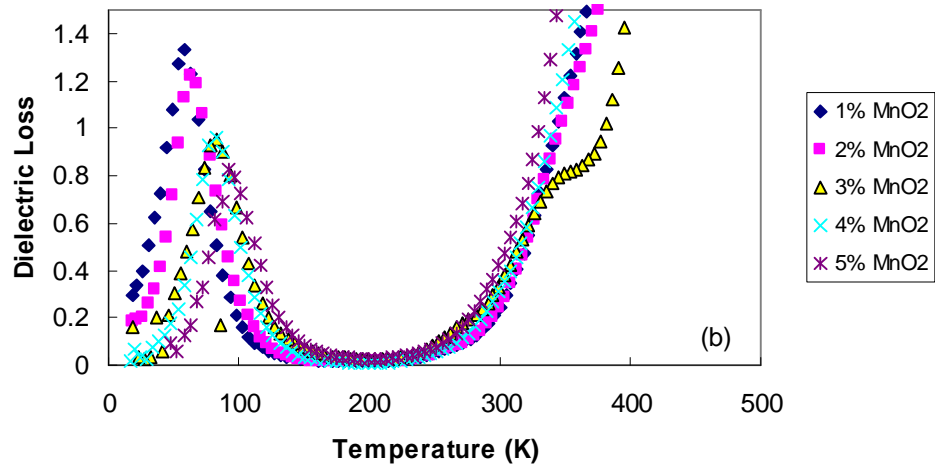
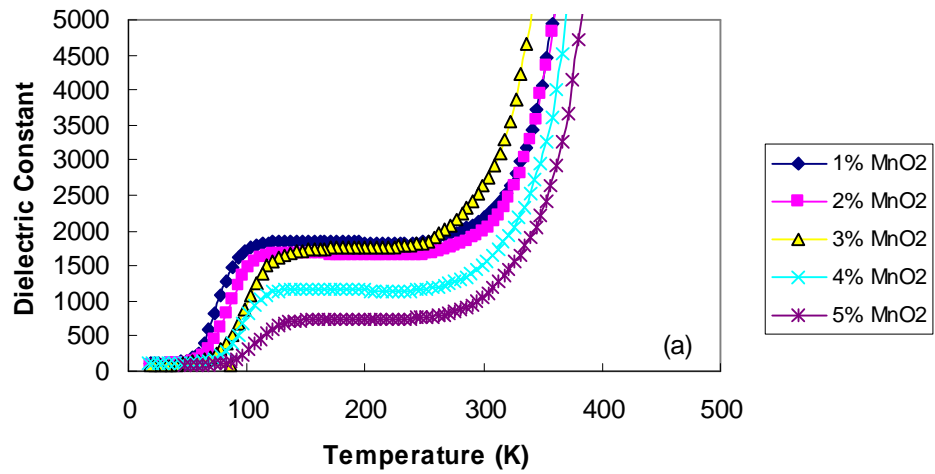


Figure 3.13 (a) (b) Temperature dependence of dielectric constant and dielectric loss of CCTO with different composition of MnO₂ additive

The profiles of the dielectric constant and loss of CCTO doped with MnO₂ are similar to the behaviors of pure CCTO. However, dopant MnO₂ greatly suppresses the dielectric constants and loss of CCTO. It is seen that the dielectric constant is further decreased with increasing MnO₂ concentration. Dielectric loss, similarly, is reduced to 0.8 for 1 kHz, which is not as obvious as incorporating with CaTiO₃. The height of the shoulder of dielectric constant and the peak of dielectric loss for different MnO₂ concentration at 1 kHz are shown in Table 3.3:

Table 3.3 Height of ϵ shoulder and $\tan\delta$ peak for different MnO₂ compositions at 1 kHz

	Height of ϵ shoulder	$\tan\delta$	
		Tm	Peak of $\tan\delta$
1% MnO ₂	1842	58.5K	1.33
2% MnO ₂	1674	63K	1.22
3% MnO ₂	1619	82.1K	0.96
4% MnO ₂	1171	82.9K	0.95
5% MnO ₂	735	93.1K	0.82

From Table 3, it can be seen that with increasing MnO₂ concentration of both the shoulder of ϵ and the peak of $\tan\delta$ are shifted to higher temperature, and their heights are suppressed. Dielectric constant and dielectric loss increase drastically for all concentrations at high temperatures above 300K. To our surprise 3% MnO₂ doping presents a second peak at around 340K, which does not exist in any other concentration.

CHAPTER IV

DISCUSSION

4.1 Pure $\text{CaCu}_3\text{Ti}_4\text{O}_{12}$ (CCTO)

4.1.1 Basic Dielectric properties of pure CCTO

CCTO displays a large dielectric relaxation process at lower than 300K, where dielectric constant decreases and the temperature of dielectric loss peak is shifted to higher temperatures with increasing frequency. In the following, we further discuss the dielectric behaviors of pure CCTO.

4.1.2 Cole-Cole plot analysis

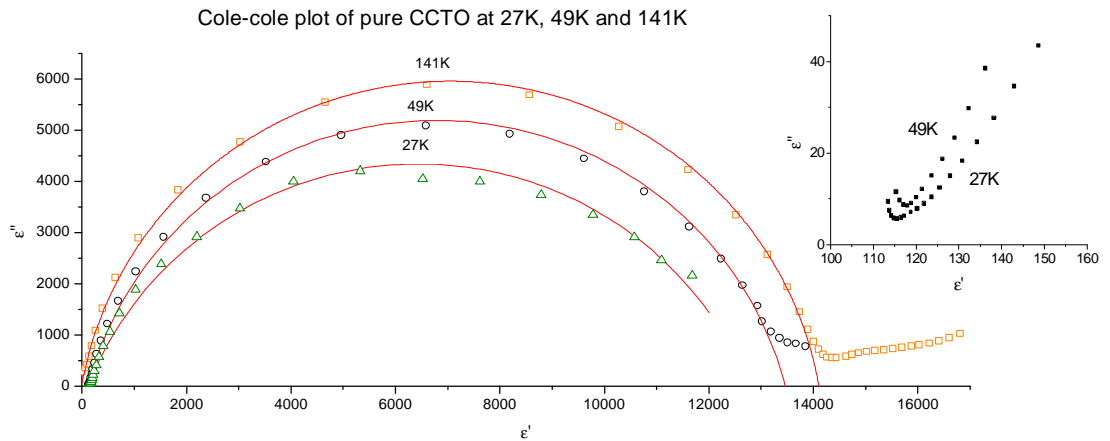


Figure 4.1 Cole-Cole plot of pure CCTO at 27K, 49K and 141K, Inset is the enlarged curves at low ϵ' , ϵ''

The imaginary part of dielectric constant, ϵ'' , can be obtained from the real part ϵ' and the dissipation factor $\tan\delta$. Considering at a certain temperature, dielectric constant varies with frequency, we could therefore plot the relation between ϵ'' and ϵ' to study the relaxation properties of a material.

The Debye Equation is widely used in this case. In Debye Relaxation Equation:

$$\epsilon^* = \epsilon_\infty + (\epsilon_0 - \epsilon_\infty)/(1 + i\omega t)$$

ϵ^* is the complex dielectric constant (where $\epsilon^* = \epsilon' - i\epsilon''$, ϵ' and ϵ'' stand for the real part and imaginary part of complex permittivity, respectively. In this text, ϵ' is sometimes written as ϵ , standing for the dielectric constant), ϵ_∞ is the permittivity at high frequency, ϵ_0 is the static permittivity, ω is the angular frequency, and t is the relaxation time. The Debye Equation gives the relation between the real and imaginary parts of permittivity by assuming all the dipoles have the same relaxation time t . Normally, the plot following the Debye Equation is a semi-circle, with radius $(\epsilon_0 - \epsilon_\infty)/2$ and center located at position $(0, (\epsilon_0 + \epsilon_\infty)/2)$. Thus by fitting the experimental data to this equation, we can obtain fitting parameters ϵ_0 , ϵ_∞ and t .

However, sometimes the curve plotted is not exactly a semi-circle, as its center is below the ϵ' axis, only less than half of a circle is shown. Considering this situation, the Debye Relaxation Equation was modified to the empirical Cole-Cole equation:

$$\epsilon^* = \epsilon_\infty + (\epsilon_0 - \epsilon_\infty)/(1 + (i\omega t)^\alpha)$$

α in this empirical equation is introduced to describe the deviation from the ideal Debye type relaxation, and in the case of $\alpha=1$, this equation becomes the same as the

Debye Relaxation Equation. This equation is now widely applied to fit experiment results.

The real (ϵ') and imaginary (ϵ'') parts of the permittivity can also be rewritten from the Cole-Cole equation in the following way:

$$\epsilon' = \epsilon_{\infty} + [(\epsilon_0 - \epsilon_{\infty})/2] \{1 - \sinh(bz) / [\cosh(bz) + \cos(bp/2)]\}$$

$$\epsilon'' = [(\epsilon_0 - \epsilon_{\infty})/2] \sinh(bp/2) / [\cosh(bz) + \cos(bp/2)] ,$$

where $b = 1 - a$, and $z = \ln(\omega t)$.

In the study of ceramic materials, this complex impedance representation of the data obtained by frequency dispersion measurements offers a graphical approach to read the type and values of each element in the equivalent circuit. This method is employed in our study to obtain a general idea of the frequency dispersive behavior of pure CCTO and how it varies with temperature.

Data measured at 27K, 49K and 141K was plotted, respectively in Fig. 4.1. It can be seen that the data fit to the Debye Equation very well. Three arcs with different radius and positions are formed for different temperatures. With increasing temperature, the radius increases and the center of the circle shifts to higher ϵ' side. This indicates that the contribution from this polarization increases with increasing temperature.

4.1.3. Relaxation times

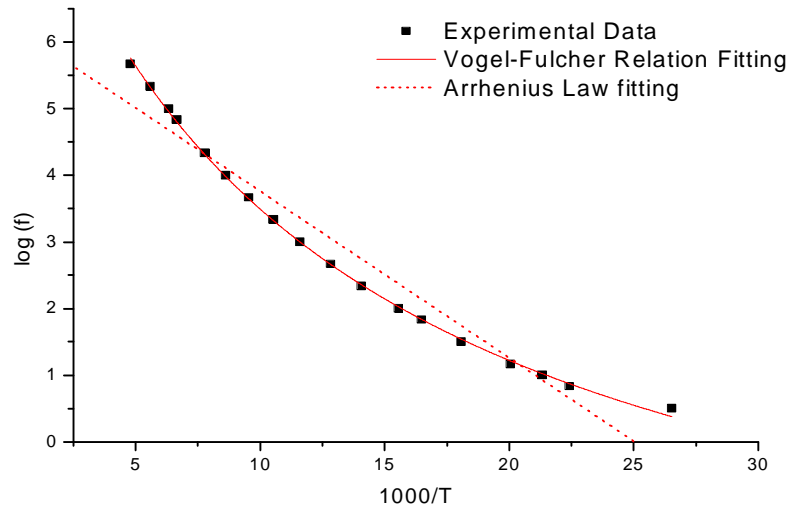


Figure 4.2 Arrhenius and Vogel-Fulcher Fitting of pure CCTO

If the dielectric relaxation is related to a thermally activated process, the relaxation rate ν will follow the Arrhenius law:

$$\nu = \nu_0 \exp[-U/(k_B T)]$$

where ν_0 is the relaxation rate at infinite high temperatures, U is the activation energy for the relaxation, $k_B = 1.38066 \times 10^{-23}$ J/K is Boltzmann's constant, and T is the absolute temperature. The temperature used in this equation is calculated from the ϵ'' vs. T plot at a certain frequency, when ϵ'' reaches its maximum.

The Arrhenius law can be rewritten in the following way:

$$\log(\nu/\nu_0) = -\frac{U}{k_B} \cdot \frac{1}{T},$$

which shows a linear relation between $\log(\nu)$ and $1/T$.

The logarithmic frequency versus reciprocal temperature for pure CCTO is plotted in Fig. 4.2. However, our attempts to fit this experimental result with Arrhenius relation failed, as the curve obviously doesn't follow a linear relation.

On the other hand, a similar equation that also describes the relation between the temperature of ϵ'' maximum and the relaxation rate is the Vogel-Fulcher relation. This relation is usually employed to describe the relaxation in spin and structural glass, written as:

$$n = n_0 \exp\{-U / [k_B (T - T_{VF})]\},$$

where T_{VF} is the Vogel-Fulcher temperature. The Vogel-Fulcher fitting to the pure CCTO experimental gives a satisfying result that is much closer to the real experimental data than Arrhenius Law (as in Fig. 4.2). However the obtained fitting parameters $U=0.126$ eV, $T_{VF}=-84$ K, $\nu_0=14.7$ kHz lack any real physical meaning. That is to say, although the Vogel-Fulcher relation presents a flawless fitting for the experimental data, it still does not give a proper explanation for the phenomena. Thus, the origin of the relaxation behavior of CCTO is still needed to be studied.

4.2 (1-y) CaCu₃Ti₄O₁₂ + y CaTiO₃

4.2.1. Characterization of (1-y) CaCu₃Ti₄O₁₂ + y CaTiO₃

These two figures (Fig 4.3 (a), (b)) are indicative of the dependence of dielectric constant and loss of CaCu₃Ti₄O₁₂ incorporating with CaTiO₃ (CCTO-CTO) on temperature at different CaTiO₃ concentration. For Fig 4 (a), as seen, 0.5, 0.8, and 0.9 shown in the graph are volume ratios. The profiles of these curves look similar: a sharp increase below 150K, a relatively flat region from 150K to 350K and a fast increase above 350K. With increasing concentration of CaTiO₃ dopant, the dielectric constant

decreases in the entire temperature range, as the dielectric constant of CTO is much lower than that of CCTO. However, below 50K the higher the CTO concentration, the higher the dielectric constant. This is because ϵ of CCTO at around 20K is 150, which is less than that of CTO, which is 250. With the increasing concentration of CTO the ϵ curve becomes. We could expect that the behavior would finally become about the same as pure CTO if keep increasing CTO concentration.

For Fig 4.3 (b), below 120K $\tan\delta$ increases quickly and a peak shows up at 120K. With increasing CTO concentration the peak is suppressed and shifted to higher temperature. From 120K to 300K $\tan\delta$ is decreased, and the higher is the CTO concentration, the faster it decreases. After 300K $\tan\delta$ starts to increase again. Note that pure and 0.5 CTO + 0.5 CCTO present a second peak at around 400K, which does not exist in 0.8 or 0.9 CCT-CT. This could be explained that with increasing CTO

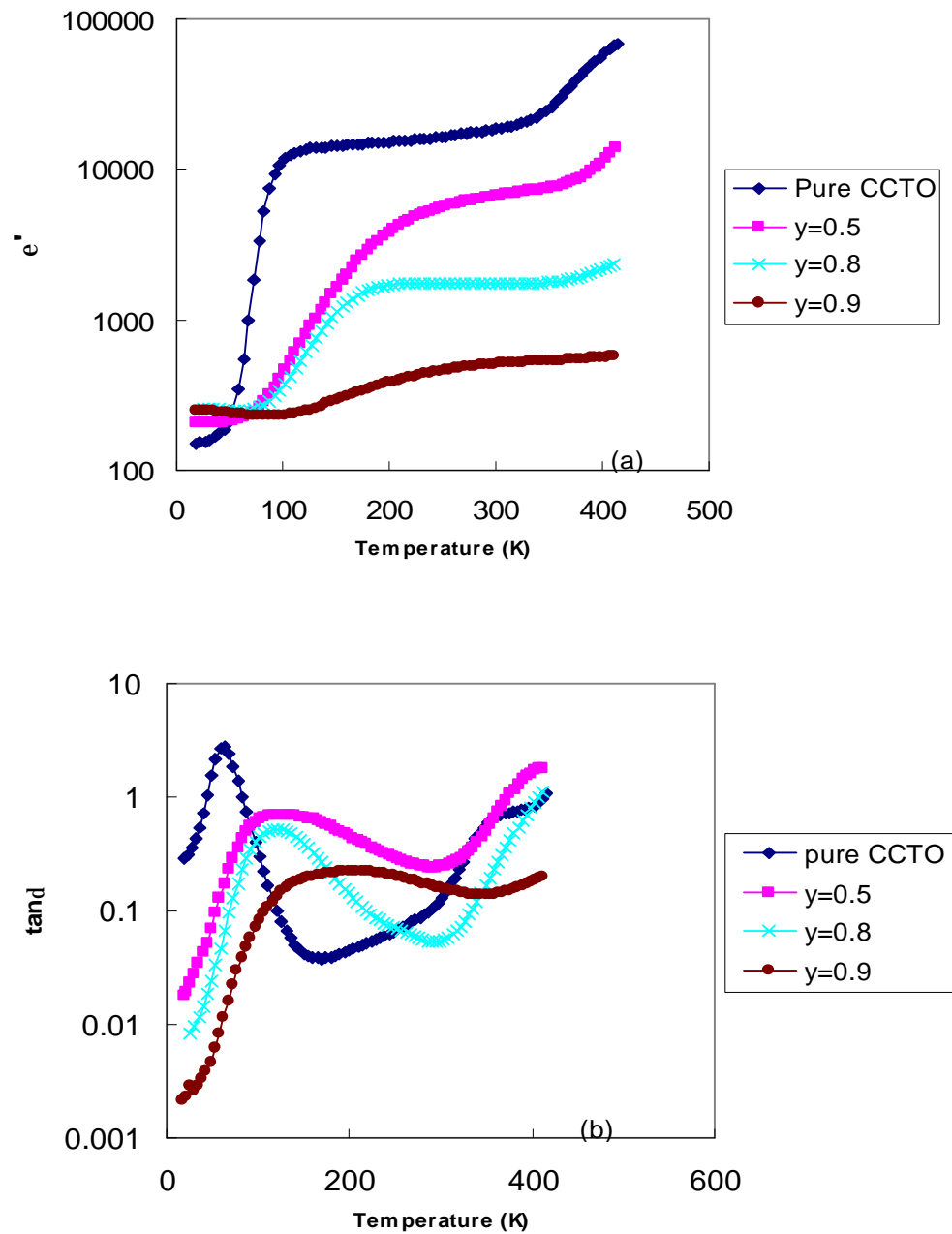


Figure 4.3 (a) (b) Dielectric constant and loss of $(1-y)$ CCTO + y CTO at 1 kHz

concentration some characteristics of CCTO are gradually suppressed and at last vanish while characteristics of CTO start to be more predominant.

4.2.2 Structure examination by X-ray diffraction

Fig. 4.4 (a) shows the X-ray diffraction pattern of pure CCTO. All peaks can be well indexed by CCTO, indicating a single phase CCTO.

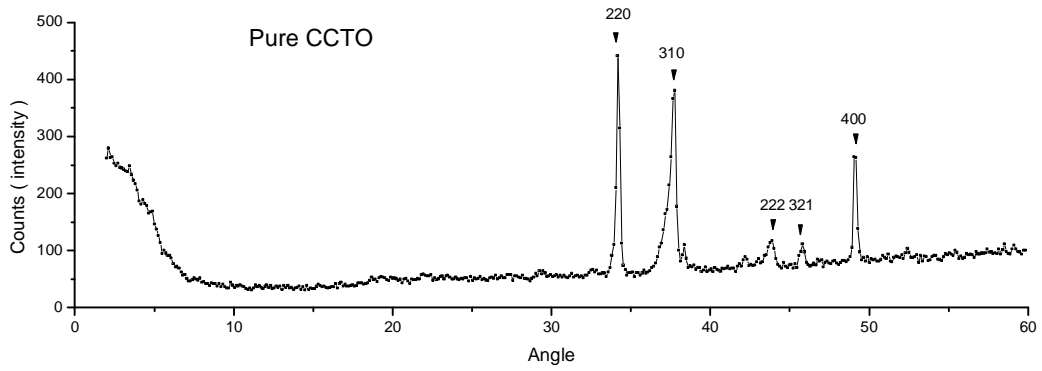


Figure 4.4 (a) X-ray diffraction pattern of pure CCTO

Figs. B and c show the X-ray diffraction pattern for $(1-y)$ CCTO + y CTO, where $y=0.33$ and 0.89 is the volume ratio. In these figures besides the peaks of pure CCTO that

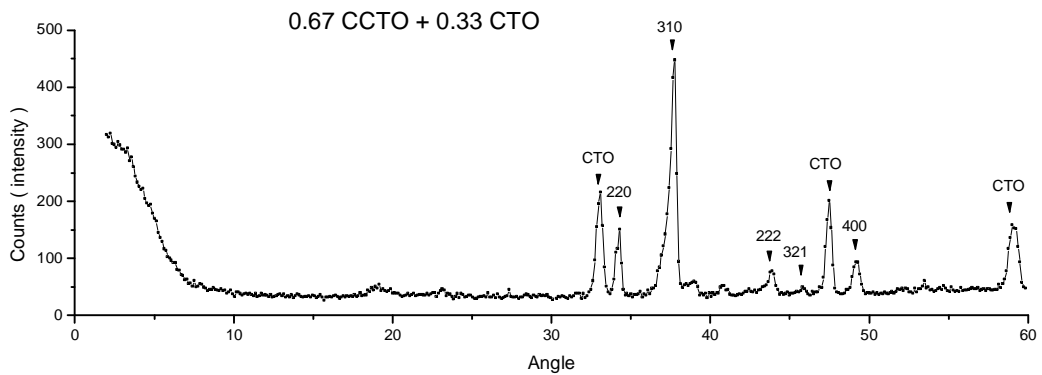


Figure 4.4 (b) X-ray diffraction pattern of 0.67 CCTO + 0.33 CTO

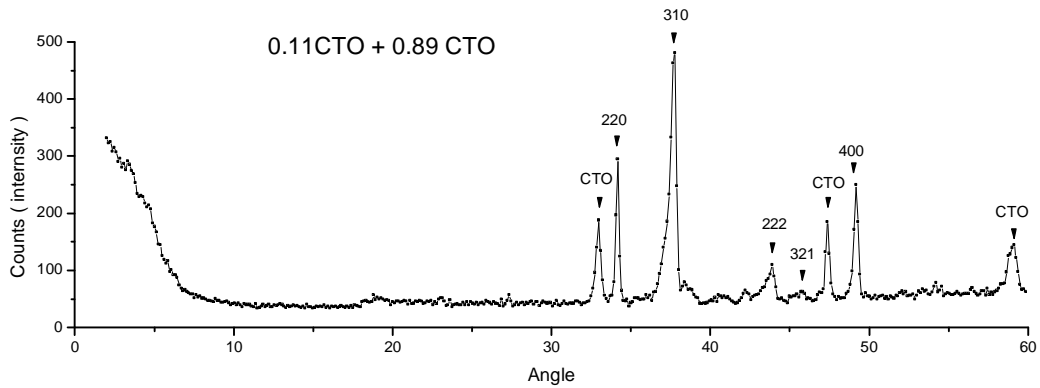


Figure 4.4 (c) X-ray diffraction pattern of 0.11 CCTO + 0.89 CTO

already shown in Fig. 1, a second set of diffraction peaks appears, which can be well indexed by CTO. This means this is a two phase material.

4.2.3 Cole-Cole plot analysis of $(1-y) \text{CaCu}_3\text{Ti}_4\text{O}_{12} + y \text{CaTiO}_3$ (volume ratio $y=0.5, 0.8$ and 0.9)

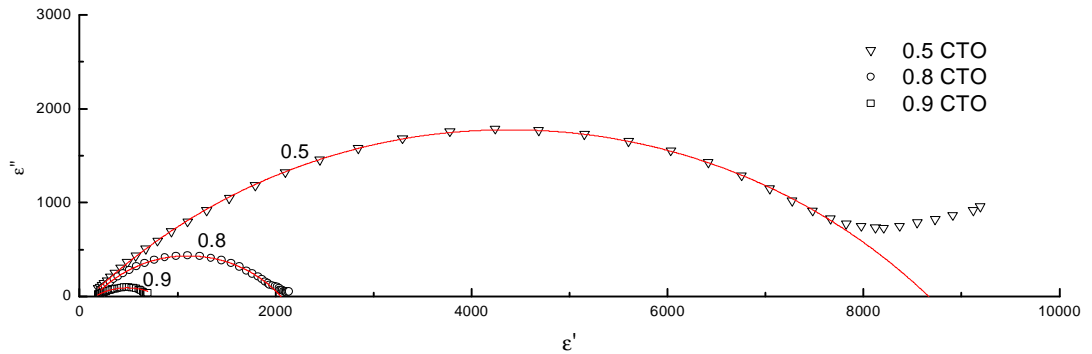


Figure 4.5 Cole-Cole plot of $(1-y) \text{CaCu}_3\text{Ti}_4\text{O}_{12} + y \text{CaTiO}_3$, volume ratio $y=0.5, 0.8$ and 0.9

As mentioned in 4.1.2, we are again using Cole-Cole plot to study the properties of $\text{CaCu}_3\text{Ti}_4\text{O}_{12}$ incorporating with different concentrations of CTO. ϵ' vs. ϵ'' of three different compositions are plotted in the Fig. 4.5 to be compared.

All three curves can be fitted with the Cole-Cole law perfectly, and the fitting parameters are shown in Table 4.1:

Table 4.1 Fitting Results of Cole-Cole plot of $(1-y) \text{CaCu}_3\text{Ti}_4\text{O}_{12} + y \text{CaTiO}_3$,
volume ratio $y=0.5, 0.8$ and 0.9

	a	e_n	e_∞
0.5 CCTO-0.5 CTO	0.771	8651	103
0.2 CCTO-0.8 CTO	0.738	2139	122
0.1 CCTO-0.9 CTO	0.729	743	167

In Table 4.1, the a parameter describes the deviation from the ideal Debye Equation and decreases slowly with increasing CTO concentration. e_0 , the static permittivity, decreases dramatically with increasing CTO concentration whereas e_∞ increases slowly. The origin of these three curves is attributed to the same polarization mechanism. In 0.5 CCTO-0.5CTO, the characteristics of CCTO predominate, which exhibit a permittivity of greater than 8600. However, as the CTO concentration increases, the permittivity is suppressed down to 2139 for 0.2 CCTO- 0.8 CTO and 743 for 0.1 CCTO- 0.9 CTO. For 0.1 CCTO-0.9 CTO, e_0 equals 743, this is much closer to the dielectric constant of pure CTO.

Hence a conclusion can be drawn that the ceramic first presents mainly the characteristics of CCTO, and as the volume ratio of CTO in the whole structure increases, characteristics of CTO gradually present themselves and predominate in the end.

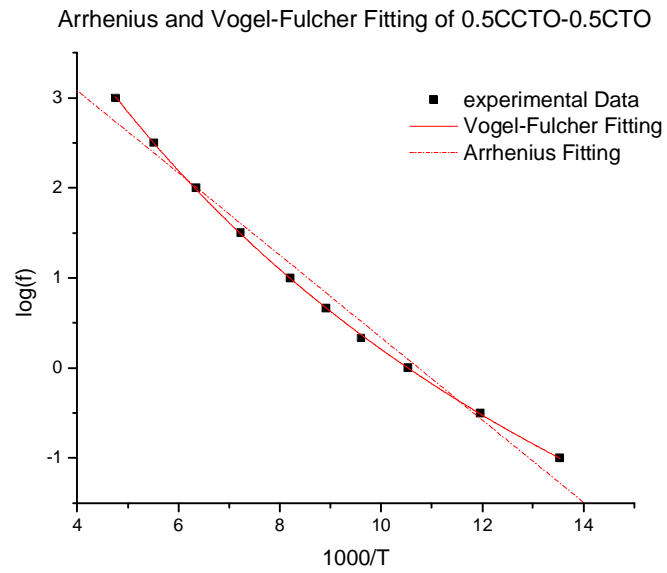


Figure 4.6 (a) Arrhenius and Vogel-Fulcher Fitting of 0.5CCTO-0.5CTO

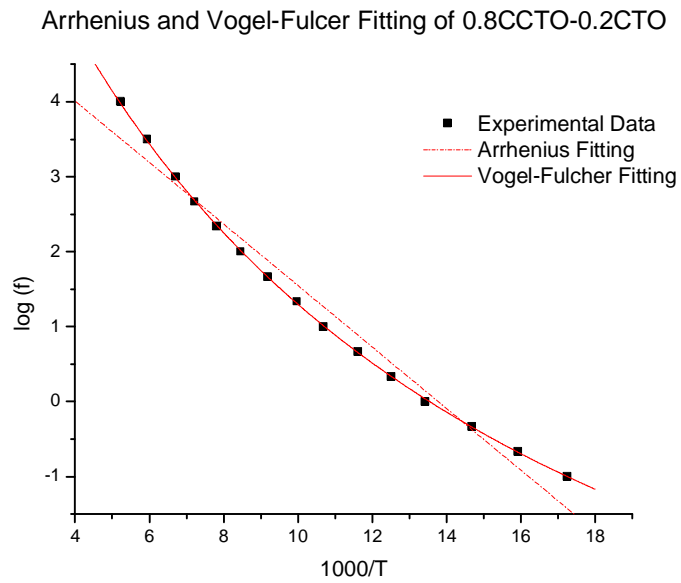


Figure 4.6 (b) Arrhenius and Vogel-Fulcher Fitting of 0.2CCTO-0.8CTO

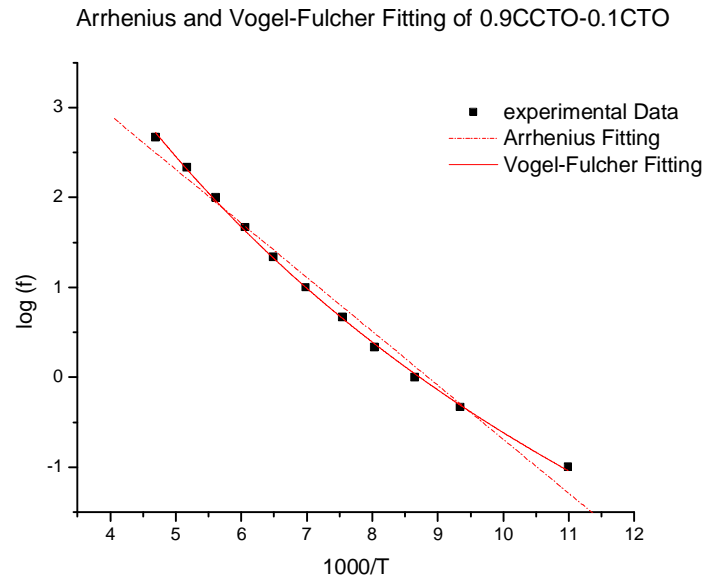


Figure 4.6 (c) Arrhenius and Vogel-Fulcher Fitting of 0.1CCTO-0.9CTO

4.2.4 Relaxation Discussion

Arrhenius and Vogel-Fulcher fitting have been carried out for (1-y) CCTO-y CTO (y= 0.5, 0.8 and 0.9). Similar results were found that all of them fit to the Vogel-Fulcher Relation rather than Arrhenius Law. An appropriate explanation to these behaviors is still being investigated.

4.2.5 Lichtenecker's Logarithmic Law

Lichtenecker's Logarithmic Law is proposed to estimate the permittivity of 2-phase materials, for example, CCTO and CTO. The equation is written as:

$$\ln \epsilon'_{cal} = y \cdot \ln \epsilon'_{CCTO} + (1 - y) \cdot \ln \epsilon'_{CTO} ,$$

where ϵ'_{CCTO} and ϵ'_{CTO} stand for the dielectric constant of pure CCTO and pure CTO, and ϵ'_{cal} stands for the dielectric constant of the mixture, y is the volume ratio that CCTO takes in the material. This theory applies with two requirements: 1. two components are

independent of each other; 2. particles of both materials distribute uniformly in the entire structure. From the X-ray diffraction experiment it was found that CCTO-CTO has a 2-phase structure exhibiting the diffraction peaks of both CCTO and CTO phase. This is clear evidence that when mixing CCTO together with CTO, they do not dissolve into each other and no new phase is created.

As long as material CCTO-CTO satisfies both requirements, the Lichtenecker's Law can be used to estimate and evaluate the experimental results. The dielectric constant of pure CTO, pure CCTO and CCTO-CTO are shown in Table 4.2:

Table 4.2 Dielectric constant of CCT-CT at 295K for 1 kHz

	Pure CCTO	0.5 CCT-CT	0.8 CCT-CT	0.9 CCT-CT	Pure CTO
ϵ'	18436	6594	1761	506	250

The fit to Lichtenecker's relation is shown in Fig. 4.7

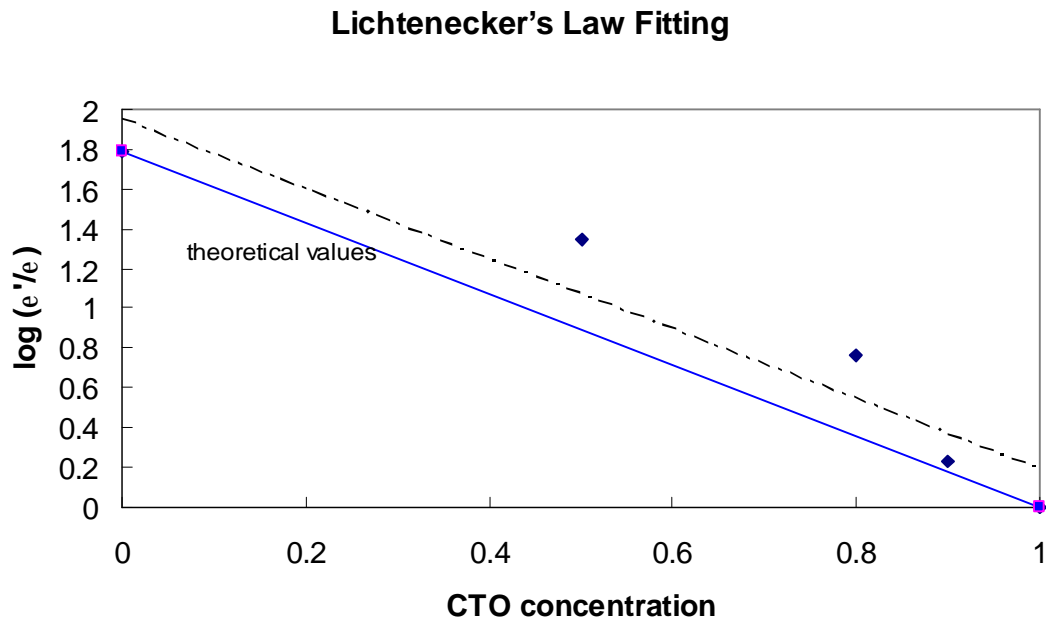


Figure 4.7 Lichtenecker's Law Fitting to pure CCTO and CCTO-CTO

As seen in Fig. 4.7 the logarithmic dielectric constant of CCTO-CTO presents an approximate linear relation with CTO concentration. The solid line in Fig. 4.7 is the theoretical values, and the dash line is the fitting to our experimental data. There is a little deviation between theoretical values and calculated values. For volume ratio $y=0.5$ and 0.8 , the real dielectric constants are larger than theoretical values.

4.3 CaCu₃Ti₄O₁₂ doped with MnO₂

4.3.1. Characterization of CaCu₃Ti₄O₁₂ doped with MnO₂

The behavior of CaCu₃Ti₄O₁₂ doped with MnO₂ is similar to that of pure CaCu₃Ti₄O₁₂, except that both dielectric constant and loss are greatly reduced. A significant decrease in ϵ' (from 15300 to 1831) is obtained when the amount of MnO₂ additive is 0.01. More MnO₂ additive continues to elicit a decrease in ϵ' . However, the ϵ' vs. MnO₂ content does not follow Lichtenecker's Logarithmic.

4.3.2. Cole-Cole plot analysis of CCTO with MnO₂ additive

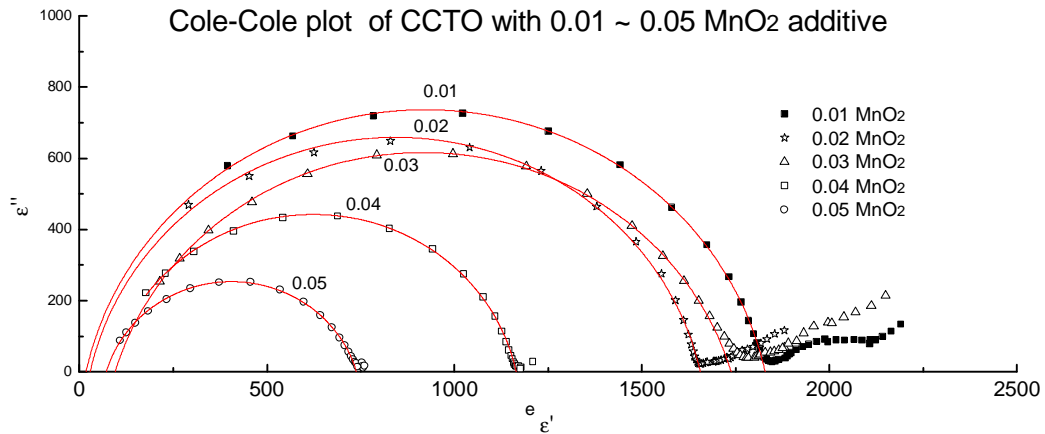


Figure 4.8 Cole-Cole plot of CCTO with 0.01 ~ 0.05 MnO₂ additive at 180K

Experimental data of CCTO with MnO₂ additive are studied and ϵ' vs. ϵ'' at 180K is plotted in Fig. 4.8. Fitting parameters are shown in Table 4.3:

Table 4.3 Fitting Results of Cole-Cole plot for CCTO with different MnO₂ additive

	$\Delta e = e_0 - e_\infty$	a	e_0	e_∞
0.01 MnO ₂	925	0.20	1828	17.5
0.02 MnO ₂	832	0.20	1656	28.2
0.03 MnO ₂	855	0.25	1738	96.1
0.04 MnO ₂	530	0.11	1158	107.9
0.05 MnO ₂	340	0.20	736	78.1

Generally the polarization strength $\Delta e = e_0 - e_\infty$ decreases with increasing MnO₂ concentration from 925 for 0.01 MnO₂ to 340 for 0.05 MnO₂. a , is between 0.11 and 0.25. Meanwhile e_0 decreases and e_∞ increases with increasing MnO₂ concentration.

For when the MnO₂ content is 0.01, 0.02 and 0.03, an additional part at the low frequency side is observed. This behavior is also present at 49K, 141K of Fig. 4.1 and 0.5 CCTO - 0.5CTO of Fig. 4.5. According to Debye Relaxation theory, every single semi-circle corresponds to a polarization mechanism. Thus, the additional part could be considered as another polarization mechanism. Therefore, this part of the curve is fitted to another circle as mechanism B, while the main semi-circle is named as mechanism A, as shown in Fig. 4.8

It is seen in Fig. 4.8 that an obvious bump exists in the range of ϵ' from 1800 to 2200, and fits to an arc pretty well, which is indicative of the existence of another polarization mechanism (mechanism B). Compared to mechanism A, Mechanism B exhibits a much smaller radius. As mentioned before, polarization strength $\Delta e = e_0 - e_\infty$ gives the contribution of a certain polarization mechanism. Therefore in Fig. 9 it is

observed that mechanism B has a value of $e_0 - e_\infty$ around 320, which is much smaller than that of mechanism A, which is around 1810.

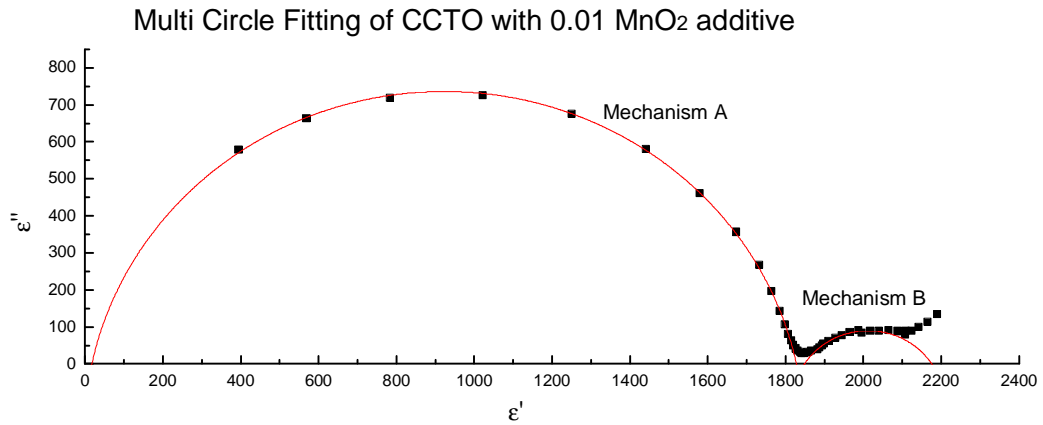


Figure 4.9 Multi Circle Fitting of CCTO with 0.01 MnO₂ additive at 180K

Greater than $e_0=2100$, it is found that ϵ'' increases again. Does this point the existence of another polarization mechanism in the higher e_0 range? These behaviors are still being studied by using first principle calculation.

CHAPTER V

CONCLUSIONS

5.1 Study of pure $\text{CaCu}_3\text{Ti}_4\text{O}_{12}$

Pure $\text{CaCu}_3\text{Ti}_4\text{O}_{12}$ (CCTO) ceramic samples were prepared via solid state reactions. The relative density of samples is of ~97%. X-ray diffraction result indicates that the samples are of single-phase perovskite structure. At room temperature, CCTO exhibits a dielectric constant of ~ 18400 and a dielectric loss of ~0.115 at 1 kHz. With increasing temperature from 20 K, the dielectric constant increases and exhibits a shoulder at ~100K, where a dielectric loss peak occurs with a peak maximum of as high as ~2.85 at 1 kHz. The complex permittivity (dielectric constant) follows the empirical Cole-Cole equation. The relaxation times follow the Vogel-Fulcher relation rather than the Arrhenius law. This is for the first time revealed in this work to my best knowledge. In addition, the resistance of the sample was also measured by the 4-probe method, the resistance first increases linearly from 735 Ωcm at 411K to $6.5 \times 10^6 \Omega\text{cm}$ at 229K then levels off from 229K to 20K. Although the pure CCTO has a huge dielectric constant as well as its weak temperature dependence, it is still not a good dielectric material for capacitance application due to its high dielectric loss and low resistivity.

5.2 Study of $(1-y) \text{CaCu}_3\text{Ti}_4\text{O}_{12} + y \text{CaTiO}_3$ (volume fraction $y= 0.5, 0.8, \text{ and } 0.9$)

The composites with compositions of “(1-y) $\text{CaCu}_3\text{Ti}_4\text{O}_{12}$ + y CaTiO_3 ” (denoted as CCTO - CTO) samples were prepared, where y is the volume fraction of CTO, and y = 0.5, 0.8, and 0.9, respectively. X-ray diffraction measurements indicate that the materials were formed by two independent phases: CCTO and CTO phases, and their intensities vary with different volume ratios. The dielectric properties of CCTO-CTO are a mixture of those of pure CCTO and CTO. With increasing CTO concentration, both the dielectric constant and dielectric loss are suppressed. The complex permittivity also follows the Cole-Cole equation, and the polarization strength is greatly decreased with increasing CTO concentration. The relaxation times follow the Vogel-Fulcher relation. For 0.5 volume ratio CTO incorporating, the dielectric loss maximum is reduced from 2.72 to 0.7 at 1 kHz while its dielectric constant is reduced from 15286 to 3831 at 200K.

5.3 Study of $\text{CaCu}_3\text{Ti}_4\text{O}_{12}$ + z MnO_2 (molar ratio z= 0.01, 0.02, 0.03, 0.04, and 0.05)

$\text{CaCu}_3\text{Ti}_4\text{O}_{12}$ doped with MnO_2 (CCTO-MnO) samples were prepared, with a compositions of “ $\text{CaCu}_3\text{Ti}_4\text{O}_{12}$ + δ MnO_2 ”, where δ is molar ratio, and δ = 0.01, 0.02, 0.03, 0.04, and 0.05, respectively. The dielectric constant is dramatically decreased from 15286 to 1831 for δ =0.01 at 200K; the dielectric loss is also greatly suppressed from 0.0447 to 0.0158.

The temperature of the dielectric loss maximum is shifted to higher temperatures with increasing MnO_2 concentration, for example, for δ =0.01 the peak is at 58.5K, and increases to 63K for δ =0.02, 82K for δ =0.03, and at last to 93K for δ =0.05. The polarization strength also decreases with increasing MnO_2 concentration, decreasing from 925 for δ =0.01 to 340 for δ =0.05.

5.4 Summary

Pure CCTO ceramic, and two series of CCTO derivatives, i.e., “ $\text{CaCu}_3\text{Ti}_4\text{O}_{12} + \text{CaTiO}_3$ ”, and “ $\text{CaCu}_3\text{Ti}_4\text{O}_{12} + \text{MnO}_2$ ” ceramics were prepared, and their phase assemblies, structure, dielectric properties, and conducting properties are studied.

The results show that incorporating with CTO or doped with MnO_2 additive, effectively decreases the dielectric loss of CCTO. This indicates that these methods are promising ways to improve the dielectric performance of CCTO-based materials for a possible practical application.

The relaxation mechanism was investigated for CCTO and its derivatives. It is for the first time revealed that the relaxation time follows the Vogel-Fulcher relation instead of Arrhenius relation. In addition, the four-probe measurement revealed the intrinsic bulk resistance.

REFERENCES

- [1] A.P Ramirez, M.A. Subramanian, M. Gardel, G. Blumberg, D. Li, T. Vogt, S.M. Shapiro. *Solid State Communications* **115** 217-200 (2000)
- [2] J. Li, M. A. Subramanian, *Chemical Materials* **33** 322 (2004)
- [3] N. Kolev, R. P. Bontchev, A. J. Jacobson, V. N. Popov, V. G. Hadjiev, A. P. Litvinchuk, M. N. Iliev. *Physical Review B* **66**, 132102 (2002)
- [4] C. C. Homes, T. Vogt, S. Shapiro, S. Wakimoto, A. P. Ramirez. *Science* **293** (2001)
- [5] D.C. Sinclair, T. B. Adams, F. D. Morrison, A. R. West. *Applied Physics Letters* **80** 12 (2002)
- [6] M. A. Subramanian, D. Li, N. Duan, B. A. Reisner, A. W. Sleight. *Journal of Solid State Chemistry* **151**, 323-325 (2000)
- [7] Eric A. Patterson. *Applied Physics Letters* **87**, 182911 (2005)
- [8] L. Feng, X. Tang, G. Cao. *Physical State solids (a)* **203**, 4, R22-R24 (2006)
- [9] J. Li, M. A. Subramanian, H. D. Rosenfeld, C. Y. Jones, B. H. Toby, A. W. Sleight. *Chemical Materials* **16**, 5223-5225 (2004)
- [10] J. Li, A. W. Sleight, M. A. Subramanian. *Solid State Communications* **135** 260-262 (2005)
- [11] W. Kobayashi, I. Terasaki. *Applied Physics Letters* **87**, 032902 (2005)
- [12] T.B. Adams, D. C. Sinclair, A.R. West, *Advanced Materials* **14**, 18 (2002)
- [13] L. He, J. B. Neaton, M. H. Cohen, D. Vanderbilt, C. C. Homes. *Physical Review B*, **65**, 214112 (2002)
- [14] P. Lunkenheimer, R. Fichtl, S. G. Ebbinghaus, A. Loidl. *Physical Review B* **70**, 172102 (2004)
- [15] M. H. Cohen, J. B. Neaton, L. He, D. Vanderbilt. *Journal of Applied Physics* **94**, 5 (2003)
- [16] G. Chiodelli, V. Massarotti, D. Capsoni, M. Bini, C. B. Azzoni, M. C. Mozzati, P. Lupotto. *Solid State Communications* **132**, 241-246 (2004)
- [17] S. Guillemet-Fritsch, T. Lebey, M. Boulos, B. Durand. *Journal of the European Ceramic Society* **26** 1245-1257 (2006)
- [18] A. Koitzsch, G. Blumberg, A. Gozar, B. Dennis, A. P. Ramirez, S. Trebst, S. Wakimoto. *Physical Review B* **65**, 052406 (2002)

- [19] Y. L. Zhao, G.W. Pan, Q.B. Ren, Y.G. Cao, L.X. Feng, Z.K. Jiao, Thin Solid Films, **445**, 7-13 (2003)
- [20] C.-F. Yang, Japan Journal of Applied Physics **35** 1806 (1996); **36**, 188 (1997)
- [21] N. Setter, R. Waaser, Acta Materials **48**, 151 (2000)
- [22] Principles of Instrumental Analysis. Fifth Edition. D. A. Skoog, F. J. Holler, T. A. Nieman
- [23] G. A. Smolenskii, V.A. Isupov, A. I. Agranovskaya, S. N. Popov, Sov. Physical Solid State **2**, 2584 (1961)
- [24] W.Si, E.M. Cruz, P.D. Johnson, P. W. Barnes, P. Woodward, and A. P. Ramirez, Applied Physics Letter. **81**, 2056 (2002)
- [25] B. Bochu, M. N. Deschizeaux, J. C. Joubert, Journal of Solid State Chemistry. **29**, 291 (1988)